Contribution of solitons to enhanced rogue wave occurrence in shallow ~~water~~depths: a case study in the southern North Sea

Ina Teutsch[1], Markus Brühl[2], Ralf Weisse[1], and Sander Wahls[2]

[1]Helmholtz-Zentrum Hereon, Max-Planck-Str. 1, 21502 Geesthacht, Germany
[2]Delft Center for Systems and Control, Delft University of Technology, 2860 Delft, South Holland, Netherlands

Correspondence: Ina Teutsch (ina.teutsch@hereon.de)

Abstract. The shallow waters off the coast of Norderney in the southern North Sea are characterised by a higher frequency of rogue wave occurrences than expected ~~according to second-order theory~~. Here, rogue waves refer to waves exceeding twice the significant wave height. The role of nonlinear processes for the generation of rogue waves at this location is currently unclear. Within the framework of the Korteweg–de Vries (KdV) equation, we investigated the discrete soliton spectra of measured time series at Norderney to determine differences between time series with and without rogue waves. For this purpose, we applied a nonlinear Fourier transform for the Korteweg–de Vries equation with vanishing boundary conditions (vKdV-NLFT). At measurement sites where the propagation of waves can be described by the KdV equation, the solitons in the discrete nonlinear vKdV-NLFT spectrum correspond to physical solitons. We do not know whether this is the case at the considered measurement site. In this paper, we use the nonlinear spectrum to classify rogue and non-rogue time series. That is, we investigate if the discrete nonlinear spectra of measured time series with visible rogue waves differ from those without rogue waves. Whether or not the discrete part of the nonlinear spectrum corresponds to solitons with respect to the conditions at the measurement site is not relevant in this case because we are not concerned with the question how these spectra change during propagation. For each time series containing a rogue wave, we were able to identify at least one soliton in the ~~discrete~~ nonlinear ~~vKdV-NLFT~~ spectrum that contributed to the occurrence of the rogue wave in that time series. The amplitudes of these solitons were ~~generally~~ found to be smaller than the crest height of the corresponding rogue wave and interaction with the continuous wave spectrum is needed to fully explain the observed rogue wave. Time series with and without rogue waves showed different characteristic soliton spectra. In most of the spectra calculated from rogue wave time series, most of the solitons clustered around similar heights, while the largest soliton was outstanding with an amplitude significantly larger than all other solitons. The presence of a clearly outstanding soliton in the spectrum was found to be an indicator pointing towards enhanced probability for ~~detecting~~the occurrence of a rogue wave in the time series. Similarly, when the discrete spectrum appears as a cluster of solitons without the presence of a clearly outstanding soliton, the presence of a rogue wave in the observed time series is unlikely. ~~Under the hypothesis that the KdV describes the evolution of the sea state around the measurement site well, t~~These results suggest that solitons and nonlinear processes substantially contribute to the enhanced occurrence of rogue waves off Norderney.

1 Introduction

Rogue waves are commonly defined as individual waves exceeding twice the significant wave height, that is the average height of the highest third of waves in a record. The occurrence of a rogue wave is a rare incident in the framework of a second-order process (Haver and Andersen, 2000). Due to their exceptional height and unexpected nature, they pose a threat to ships and offshore platforms (Bitner-Gregersen and Gramstad, 2016). Rogue waves have not only been observed in the deep and shallow water depths of the ocean, but also approaching coastlines (Didenkulova, 2020). There has been a lively discussion on whether the occurrence frequency of rogue waves in the open ocean is well described by ~~second-order models~~common wave height distributions. Both Rayleigh (Longuet-Higgins, 1952) and Weibull distributions (Forristall, 1978), which are based on the linear superposition of wave components, have been used to describe the distributions of wave and crest heights. Later theories include second-order steepness contributions in wave height distributions (e.g., Tayfun and Fedele, 2007). Distributions were assessed for measurement data collected by surface-following buoys (e.g., Baschek and Imai, 2011; Pinho et al., 2004; Cattrell et al., 2018), by radar devices (e.g., Olagnon and v. Iseghem, 2000; Christou and Ewans, 2014; Karmpadakis et al., 2020), and laser altimeters (e.g., Soares et al., 2003; Stansell, 2004), as well as by ADCPs (Fedele et al., 2019). Independent of the measurement device, some authors found measured wave heights to agree well with the established distributions (e.g., Casas-Prat et al., 2009; Waseda et al., 2011; Christou and Ewans, 2014), while others found the frequency of rogue wave occurrences over-estimated (e.g., Olagnon and v. Iseghem, 2000; Baschek and Imai, 2011; Orzech and Wang, 2020) or underestimated (e.g., Stansell, 2004; de Pinho et al., 2004). ~~For example, for the northern North Sea, all three inferences have been made: While Olagnon and v. Iseghem (2000) found rogue wave occurrences to be overpredicted by the classical distributions, they appeared to be in agreement with a Weibull distribution in data of Waseda et al. (2011) and to be underestimated in the dataset of Stansell (2004). Rogue wave occurrences in buoy data from the US coast, recorded in shallow, intermediate and deep water, were found to be strongly overestimated by a Rayleigh distribution. Furthermore, the respective~~ Numerous authors describe local differences in rogue wave occurrence frequency between their measurement stations (Baschek and Imai, 2011), depending on the wave climate (Stansell, 2004) and especially in coastal waters, where waves interact with the seabed (Cattrell et al., 2018; Orzech and Wang, 2020). Massel et al. (2017) stated that the wave height distribution is dependent on the water depth, which, however, is not explicitly included in the common models. Karmpadakis et al. (2020) found that while different models can describe wave height distributions well within narrow ranges of sea state conditions, no model is able to describe measured wave heights for a wide range of sea states accurately. Mendes and Scotti (2021) recently introduced a new exceedance probability distribution for rogue waves by geometrically combining some commonly used distributions. The combined distribution is more flexible than the individual distributions, as it is additionally dependent on sea state variables. The distribution is capable of describing rogue waves in a wide range of sea states and able to describe the uneven rogue wave distributions in storms that were observed by Stansell (2004).

In a previous study, we have analysed measurement data from various stations in the southern North Sea (Teutsch et al., 2020) and found rogue wave frequencies to vary spatially and by measurement device. For data obtained from wave buoy measurements, we generally found rogue wave frequencies slightly overestimated by the Forristall distribution, which is a special form of the Weibull distribution, fit to wave data recorded during hurricanes (Forristall, 1978). An exception was one

measurement buoy, which was located in the shallow waters off the coast of the island Norderney, Germany (Fig. 1). For this buoy, enhanced rogue wave occurrence was observed, which could not be explained by the Forristall distribution~~, was observed~~. This suggests that nonlinear processes and interactions may play a role in ~~explaining the increase in~~increasing the rogue wave occurrence frequency at this specific location.

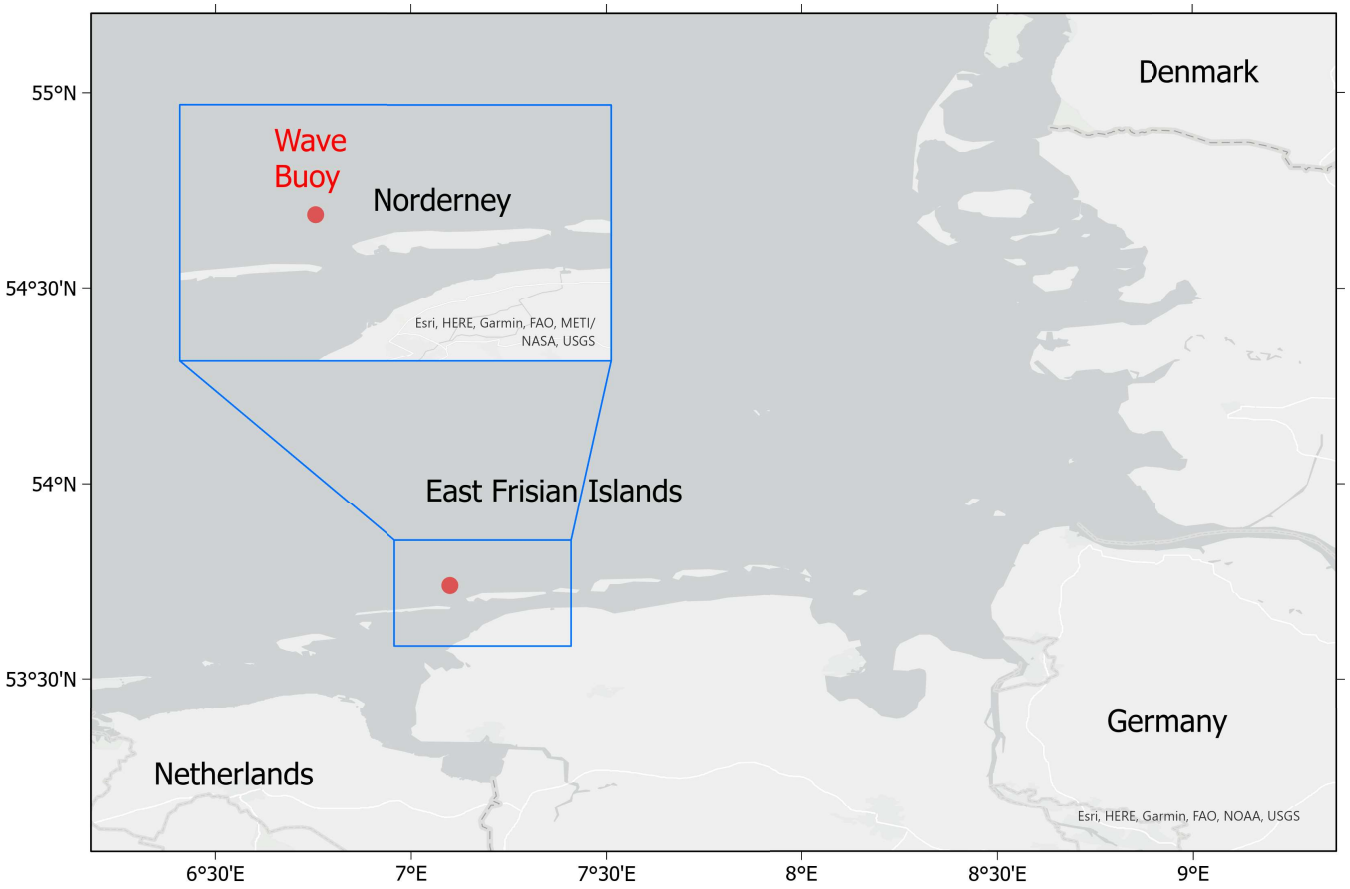

Figure 1. Map of the German Bight, showing the location of the measurement buoy close to the island Norderney.

So far, the nonlinear behaviour of deep-water rogue waves has received considerably more attention than that of shallow-water rogue waves. The evolution of the complex envelope of unidirectional wave trains in deep water can be described by the cubic nonlinear Schroedinger (NLS) equation (Onorato et al., 2001; Slunyaev, 2005). ~~Deep water in this context is defined in terms of the wave number k and the water depth h as $k\,h > 1.36$, which represents the lower limit for the application of the NLS equation (Osborne, 2010).~~ The NLS equation is a weakly nonlinear, narrow-banded approximation of the fully nonlinear water wave equations, including both nonlinearity and dispersion (Serio et al., 2006). In deep water, rogue-wave occurrence beyond the second-order model has been explained, for example, by a nonlinear instability that was also found in numerical simulations and tank experiments (Dysthe et al., 2008). Here, uniform wave trains are modulationally unstable to small ~~oblique~~side-band perturbations and disintegrate

into groups, in which the highest wave becomes significantly larger than the wave height in the original train (Benjamin and Feir, 1967). This nonlinear focusing mechanism does not only increase the maximum wave height, but also the probability of rogue wave occurrence (Slunyaev and Shrira, 2013). Alber (1978) derived a stability criterion for such narrow-banded random waves, which was introduced as a parameter for the characterisation of wave nonlinearity by Onorato et al. (2001) and later became known as the Benjamin-Feir index (BFI) (Janssen, 2003). A large BFI corresponds to enhanced ~~nonlinearity~~nonlinear processes (de León and Soares, 2014) and has been suggested as an indicator for enhanced rogue wave probability in deep water (Gramstad and Trulsen, 2007). The NLS equation has some exact solutions (known as breathers) that ~~explain~~describe the dynamics of the modulational instability~~, which~~. Breathers have been suggested as an analytical model of rogue waves in a unidirectional case (Dysthe and Trulsen, 1999). Here a uniform wave train develops into a number of breathers, and then relaxes back to a uniform wavetrain (Clamond et al., 2006; Gramstad and Trulsen, 2007). Each breather solution represents the modulational instability growth for a specific initial perturbation.

A nonlinear Fourier transform (NLFT) method has been developed that is able to identify the composition of surface elevation time series in terms of linear waves, Stokes waves and breathers (Osborne, 2010). The author characterises a sea state with a breather-dominated spectrum as a "rogue sea" condition. The method has been applied to describe the composition of real ocean data (Osborne et al., 2019). In the framework of the NLS equation, a large part of the dynamics of nonlinear waves can be described in terms of interacting breathers (Slunyaev and Shrira, 2013). Specifically the Peregrine breather (Peregrine, 1983), which is characterised by only one oscillation in time and an amplitude of three times the initial wave train, has been subject to analysis (Shrira and Geogjaev, 2010). Recently, the growth of crest heights due to nonlinearities that was observed in deep water, has been extended to intermediate water depths (Karmpadakis et al., 2019). However, the relevance of the modulational instability of the NLS equation to the formation of real rogue waves remains unclear because most of these works only consider the specific scenario of perturbed plane wave envelopes (Slunyaev and Shrira, 2013). Recent studies have come to the conclusions that the modulational instability is not the main generation mechanism of rogue waves in real ocean time series (Fedele et al., 2016) and that the BFI is a weak predictor for real-world rogue wave risk (Haefner et al., 2021).

In addition to the investigations on the modulational instability, deep-water envelope solitons have been in focus with regard to a possible connection with rogue wave occurrence. Slunyaev (2006) investigated rogue waves in deep water in measurement records. By solving the scattering problem in the approximation of the NLS equation, the nonlinear dynamics of an envelope soliton was investigated to predict possible rogue wave events. The NLS equation was used as an approximate model of the wave dynamics. The procedure is a method to detect envelope solitons and estimate their parameters like amplitude, velocity and position. Slunyaev (2018) estimated the accuracy of this procedure for strongly nonlinear waves. The NLFT was applied to the interpretation of deep-water waves, the extraction of soliton-like groups and the prediction of their further dynamics. Carrying this work further, Slunyaev (2021) identified a wave group in numerical simulations as a stable envelope soliton, which could be related to rogue wave events. Onorato et al. (2021) reported on the observation of a wave packet in strongly nonlinear waves in the Atlantic ocean. While assuming that the dynamics of the wave packet, at least for short time and space, could be described by the NLS equation, they applied the NLFT to establish the nonlinear contents of the wave packet.

The role of ~~nonlinearity~~nonlinear processes with respect to rogue wave generation in shallow water has received considerably

less attention than for deep water. Shallow-water wind waves substantially differ from deep-water wind waves and it is not appropriate to simply scale the deep-water nonlinear interaction to shallow-water waves (Janssen and Onorato, 2007). Shallow water in the context of the KdV equation is defined in terms of the wave number k and the water depth h as $kh \leq 1.36$ (Osborne and Petti, 1994, p. 1731; Osborne, 1995, p. 2629). As the water depth becomes more and more shallow, a wave-induced current develops and less wave energy is available for nonlinear focusing (Benjamin and Feir, 1967; Janssen and Onorato, 2007). Although waves in shallow water can also destabilise due to oblique perturbations (Toffoli et al., 2013), the modulational instability in shallow water does not enhance the formation of extreme waves (Fernandez et al., 2014). Didenkulova et al. (2013) supported by observations that the influence of the modulational instability on rogue wave generation becomes less probable in shallow water. Fedele et al. (2019) stated that waves in shallow water break before they can start to "breathe" and become rogue waves. Already Glukhovskiy (1966) expected high individual waves in shallow water to occur less frequently than predicted by the Rayleigh distribution, due to depth-induced wave breaking. Therefore, some authors expect the rogue wave probability to decrease in shallow water (e.g., Slunyaev et al., 2016). Other authors ~~refer~~referred to the large ratio between nonlinearity and dispersion in shallow water (Kharif and Pelinovsky, 2003) and concluded that Gaussian statistics are not sufficient for the description of shallow-water waves and that rogue waves are likely to occur more frequently as the water depth decreases (Garett and Gemmrich, 2009; Sergeeva et al., 2011). ~~While in deep water only the free-surface nonlinearity must be taken into account, t~~The ~~nonlinearity~~nonlinear processes in shallow water ~~is~~are mainly a result of the interaction of waves with the sea floor (Prevosto, 1998). Refraction, shoaling and higher-order nonlinear effects change the shapes of waves and their energy spectrum (Bitner, 1980; Tayfun, 2008). ~~However, so far only few studies have addressed the impact of bathymetry on rogue wave generation. For example,~~ Soomere (2010) found that in shallow water, compared to deep water, due to wave-bathymetry interaction, additional processes associated with the generation of extreme waves, like wave amplification along certain coastal profiles, redirection of waves or the formation of crossing seas, are relevant, and therefore more rogue waves should be expected in nearshore regions. ~~The shallow-water equivalent to the NLS equation is the Korteweg–de Vries (KdV) equation (Korteweg and de Vries, 1895).~~In shallow water, the wave evolution is described by the Korteweg–de Vries (KdV) equation (Korteweg and de Vries, 1895). It describes weakly nonlinear and dispersive progressive unidirectional free-surface waves in shallow water with constant depth (Peregrine, 1983). Shallow-water waves in this work are defined as $kh \leq 1.36$, which represents the upper limit for the application of the KdV equation (Osborne and Petti, 1994; Osborne, 1995). The solutions of the KdV are stable, in that the wave amplitude does not alter significantly when the initial wave train is perturbed. This is the mathematical explanation of why rogue waves in shallow water cannot be a result of the modulational instability. The inverse scattering transform (IST) was introduced as a tool to solve the KdV equation (Gardner et al., 1967), and later-on also a broader range of evolution equations (Ablowitz et al., 1974). The name scattering transform has its roots in physics, where the tools applied in the derivation of the IST are used to analyse how particles behave in the interaction with a scatterer (Wahls and Poor, 2015). When a time series is close to linear, its scattering data essentially reduces to the linear Fourier ~~T~~transform (FT). Therefore, the IST has been called a "natural extension of Fourier analysis to nonlinear problems" (Ablowitz et al., 1974). Henceforth in this paper, the method is referred to as the nonlinear Fourier transform for the KdV equation (KdV-NLFT). Zabusky and Kruskal (1965) discussed, by numerically solving the KdV equation, the decomposition of a~~n initial~~ cosine signal into a train of eight solitons. They first documented that the size

and shape of solitons remain unaffected by nonlinear interactions with each other. Hammack and Segur (1974) showed by comparison with observations in a wave tank that the asymptotic behaviour of waves in shallow water is well described by the KdV equation. Ablowitz and Kodama (1982) confirmed by analysing the long time asymptotic solution of the KdV equation, that solitons interact elastically with other solitons and also with the dispersive wavetrain. Osborne and Bergamasco (1986) applied the NLFT for the KdV equation and found the results of Zabusky and Kruskal (1965) on soliton interaction confirmed for periodic boundary conditions. Osborne et al. (1991) showed for periodic boundary conditions that solitons are hidden in measurement time series, which can be found by solving the KdV equation by the NLFT. Costa et al. (2014) found a method to filter soliton trains from measurement data by a linear Fourier transform for the KdV equation with periodic boundary conditions and associating them with wave packets. Giovanangeli (2018) determined the solitons hidden in a random wave field in shallow water by the NLFT for the KdV equation. They established histograms of solitons as a function of their amplitudes at different observation points. They investigated the relation between the soliton and the oscillatory wave components, as to conclude on the energy distribution in the random wave field. Brühl and Oumeraci (2016) confirmed in laboratory experiments and numerical simulations that long cosine waves in very shallow water are unstable in the following sense. They decompose into trains of solitons that are solutions to the KdV equation and that show larger amplitudes than the initial wave height. While the time series changes with time, the nonlinear amplitude spectrum remains invariant. The KdV-NLFT yields a discrete set of eigenvalues and a continuous spectrum. Each of the eigenvalues corresponds to a soliton (Peregrine, 1983), and the continuous spectrum to oscillatory waves. The asymptotic development of the solution with time leads to a decay of the oscillatory part and the solitons asymptotically dominate the solution ~~(Zabusky and Kruskal, 1965)~~(Ablowitz and Segur, 1981, Chapter 1.7c).

The nonlinear interaction of solitons in shallow water has been discussed with regard to its role in rogue wave generation. Based on the KdV-NLFT, Pelinovsky et al. (2000) showed that dispersive focusing is possible in the nonlinear case, ~~given~~but mentioned that "the "nonlinear" [wave] train ~~includes at least one~~should include a soliton" (Pelinovsky et al., 2000). Equivalently to the linear case, in which rogue waves evolve from the superposition of wave components, nonlinear focusing is then the interaction between one or, in principle, multiple solitons with ~~oscillatory~~dispersive waves, due to their velocity difference. For the unidirectional case, several authors (Kharif and Pelinovsky, 2003; Soomere and Engelbrecht, 2005) found that the interaction of KdV solitons does not lead to a significant increase in surface elevation. Soomere (2010) considered that since soliton interaction in the unidirectional case does not lead to an enhancement in surface elevation, a higher nonlinearity should even lead to a decrease in rogue wave occurrence probability. Since this is not consistent with observations, he concluded that directionality must play a role for the rogue wave generation in shallow water. Indeed, crossing solitons are known to be able to produce large amplitudes (Peterson et al., 2003). Zakharov and Shabat (1975) found the analytical two-soliton solution of the Kadomtsev-Petviashvili (KP) equation describing this case. Hammack et al. (1989) investigated two long-crested solitary waves propagating in different directions and interacting. In contrast to linear superposition, the interaction of two crossing solitons may produce a crest up to four times higher than the incoming waves (Peterson et al., 2003). Peterson et al. (2003) discussed the interaction of shallow-water solitons against the background of heavy fast ferry traffic. They made this restriction because shallow-water areas with heavy ship traffic are more likely to produce regular, long-crested 2D wave trains, necessary for their model of rogue waves, than wind sea on the open ocean. They emphasised that the interaction area is restricted and it

is unlikely to detect ~~an interaction soliton~~soliton interaction in one-point in-situ measurements. ~~Osborne et al. (1991) analysed nearly unidirectional shallow-water measurement data from the Adriatic Sea in the framework of the KdV equation for an IST with quasi-periodic boundary conditions. They found several solitons in the discrete spectrum of the IST and pointed out their physical relevance for the structure of the time series.~~

Since rogue wave occurrence in shallow water that goes beyond second order has not been sufficiently explained, and almost all investigations in previous work are based on theoretical considerations, numerical simulations or laboratory experiments, we consider real measurement time series in the framework of the KdV equation. We expand the investigation of data measured by a surface-following buoy off the coast of Norderney in the southern North Sea, for which ~~second-order distributions~~wave height distributions based on linear superposition have been shown to underestimate rogue wave occurrence (Teutsch et al., 2020). Our study is based on the insight that oscillatory waves in sufficiently shallow water decompose into separate solitons (Zabusky and Kruskal, 1965; Brühl and Oumeraci, 2016). Osborne and Bergamasco (1986) showed that the solitons that are hidden in a time series may be found by computing an NLFT spectrum. In our study, we ~~We~~ obtain a discrete soliton spectrum from the nonlinear Fourier transform for the KdV equation with vanishing boundary conditions (vKdV-NLFT) ~~and~~. We apply vKdV-NLFT as a spectral analysis method to explore to what extent the presence of solitons might contribute to ~~this~~the enhanced ~~statistical~~ rogue wave occurrence off Norderney. For this purpose, we compare the soliton spectra of samples with and samples without rogue waves. Following Sugavanam et al. (2019), we use the NLFT as a signal processing tool. Our goal is to classify time series by their nonlinear spectra. We do not assume that the nonlinear soliton spectra remain constant during propagation beyond the measurement site, which would be the case only if the propagation conditions are well approximated by the KdV equation. The paper is structured as follows. Section 2.1 describes the measurement site and the dataset and gives a definition for rogue waves. In Sect. 2.2, the application of vKdV-NLFT to the measurement data is explained. Sect. 3 consists of two parts. In Sect. 3.1, we explore the direct association of solitons calculated from NLFT with rogue waves, while Sect. 3.2 discusses statistical differences in the soliton spectra of time series with and without rogue waves. In Sect. 4, we discuss the time windows and location for which our results are valid, and suggest further investigations. In Sect. 5 our conclusions are presented.

2 Methods

2.1 Measurement site and dataset

We analysed wave elevation data measured by a surface-following buoy off the coast of the island Norderney in the German Bight in the time period between 2011 and 2016. The measurement buoy was deployed at a nominal water depth of $h = 10$ m, which was assumed to be constant for the following analyses. Actually, the water depth off the coast of Norderney is not constant, as the bathymetry at the location is spatially highly variable with strong gradients (Fig. 2). ~~The buoy is located right above a steep slope, running perpendicular to the mean incoming wave direction (Fig. 3).~~The bed slope perpendicular to the wave direction varies between 1:500 (offshore direction) and 1:200 (onshore direction). Since the buoy is restricted only by its mooring, it has the possibility to move horizontally. The actual water depth h below the horizontally moving buoy may then be subject to rapid changes. In addition, the tidal range at the site is about 2.5 m (NLWKN, 2021), which further causes the water depth to vary.

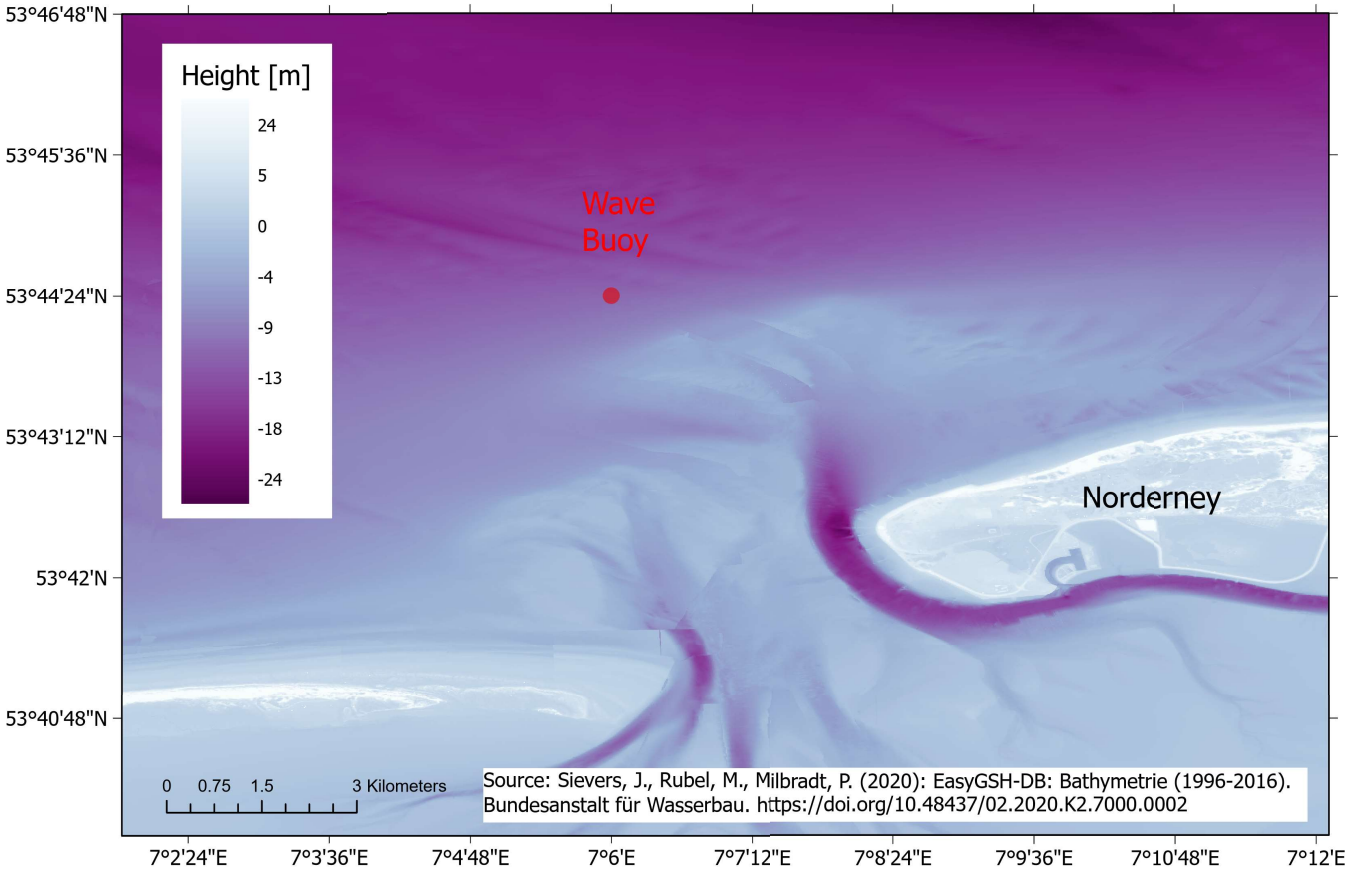

Figure 2. Bathymetry conditions [NN+m] at Norderney and the position of the measurement buoy.

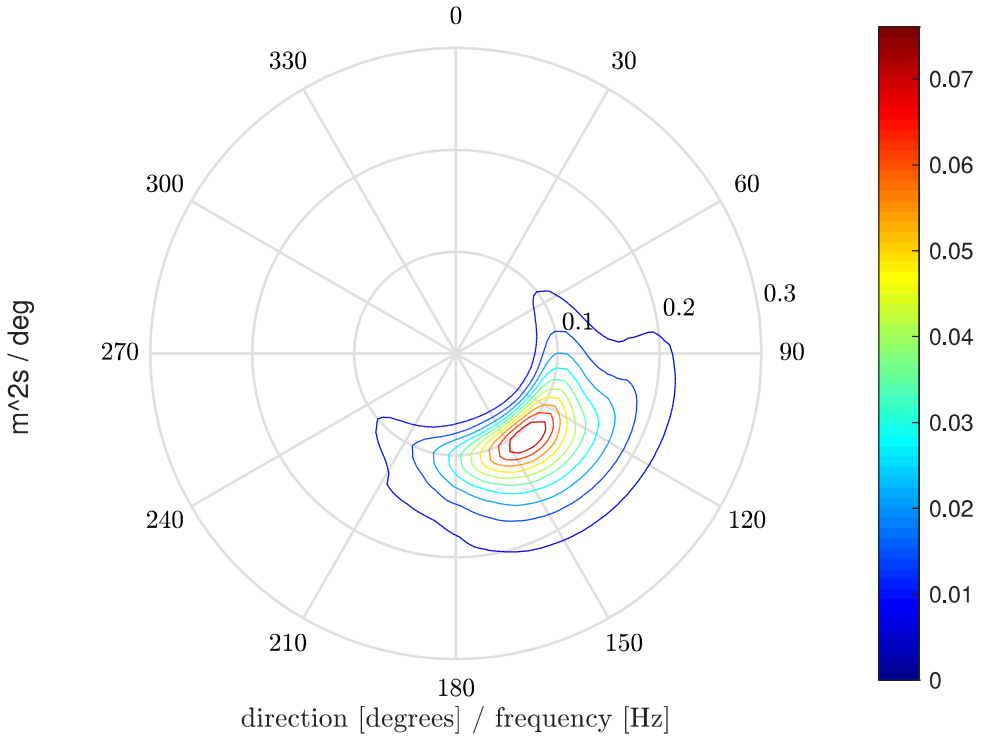

Figure 3. Mean directional wave spectrum from the time period 2011-2016, obtained by use of DIWASP (Johnson, 2002).

The wave data were measured at a frequency of 1.28 Hz and are available as a set of time series (samples) of 30 minute length. To exclude low-energy sea states in the following, only samples with a significant wave height H_s above the long-term 70th percentile of the significant wave height, $H_{s,70} = 1.29$ m, were included in the analysis. The significant wave height H_s is here defined as the mean of the highest 30 % of the wave heights in a 30 minute sample. $H_{s,70}$ was calculated from the significant wave heights H_s of all 30 minute samples during the six years of available measurement data. On the one hand, this excludes possible measurement uncertainties caused by ~~small~~short waves that are only described by a few points, and on the other hand, it includes only rogue waves of heights relevant for offshore activities. Since the KdV equation for shallow water was to be applied to the data, only samples satisfying shallow-water conditions in terms of the validity of the KdV equation were included in the study. The definition of shallow water depths for the applicability of the KdV equation is different from the commonly used definition of shallow water in the engineering context, $kh < \pi/10$ (Dingemans, 1997). The shallow-water condition used in this study was (Osborne and Petti, 1994, p. 1731; Osborne, 1995, p. 2629)

$$\frac{h}{L} < 0.22 \text{ or } kh \leq 1.36 \tag{1}$$

with water depth h and wavelength L. The wavelength was calculated as

$$L = T_p * c \tag{2}$$

from the peak period $T_p = f_p^{-1}$ of each sample, with f_p the peak frequency in the linear fast Fourier transform (FFT) spectrum of the sample, and the ~~shallow-water wave celerity~~linear phase speed $c = \sqrt{gh}$ with gravity g. Following Eq. (1) and Eq. (2), the condition for the peak period may be written as

$$T_p > \frac{h}{0.22 \cdot c}. \tag{3}$$

For a water depth of $h = 10$ m, the peak period thus had to satisfy the condition $T_p > 4.6$ s, in order for a sample to classify for shallow-~~water~~depth conditions, in which the KdV equation is valid. We based the shallow-water condition on the peak period T_p of the entire sample to assume that shallow-water wave properties as described by the KdV equation strongly contribute to the wave processes in the sample. Nevertheless, it was additionally ensured that each of the individual rogue waves (or the highest wave in each sample that did not contain a rogue wave) satisfied ~~shallow-water~~the depth conditions required for the applicability of the KdV equation, based on its period $T_{\max}$. Of all the selected samples above $H_{s,70}$, ~~shallow-water~~the required shallow depth conditions applied in more than 98 % of the cases and were thus the dominant condition in these samples. The 2 % of the samples not satisfying ~~shallow-water~~the condition~~s~~of shallow depth were discarded and not considered in the analysis. In the considered samples, kh ranged between 0.38 and 1.36.

Rogue waves are commonly defined as waves with an individual height H from crest to trough of (Haver and Andersen, 2000)

$$H \geq 2.0\ H_s \tag{4}$$

and/or waves with a crest height C above still water level of (Haver and Andersen, 2000)

$$C \geq 1.25\ H_s. \tag{5}$$

In a previous study based on measurement data from the southern North Sea (Teutsch et al., 2020), we found that the rogue wave frequency significantly deviated from the Forristall distribution for wave heights larger than $2.3\ H_s$. Therefore, in the present study we further define "extreme rogue waves" by a more strict height criterion of

$$H \geq 2.3\ H_s. \tag{6}$$

For the definition of a wave, the zero-upcrossing method was used.

The measured time series were subdivided into five categories:

"~~normal~~non-rogue samples"- measurement samples that did not include any rogue wave.

"height rogue samples"- measurement samples that include a rogue wave only according to the height criterion defined in Eq. (4), while excluding the extreme rogue waves according to Eq. (6) and excluding the double rogue samples (see below).

"crest rogue samples"- measurement samples that included a rogue wave only according to the crest criterion defined in Eq. (5), while excluding the double rogue samples.

"double rogue samples"- measurement samples that included a rogue wave ~~according to~~that fulfilled both the criteria defined in Eq. (4) and Eq. (5) at the same time, while excluding the extreme rogue waves according to Eq. (6).

"extreme rogue samples"- measurement samples that included a rogue wave according to the height criterion defined in Eq. (6), while excluding the double rogue samples.

Examples of each time series category are shown in Fig. 4. Table 1 shows the number of samples and its percentage in each category.

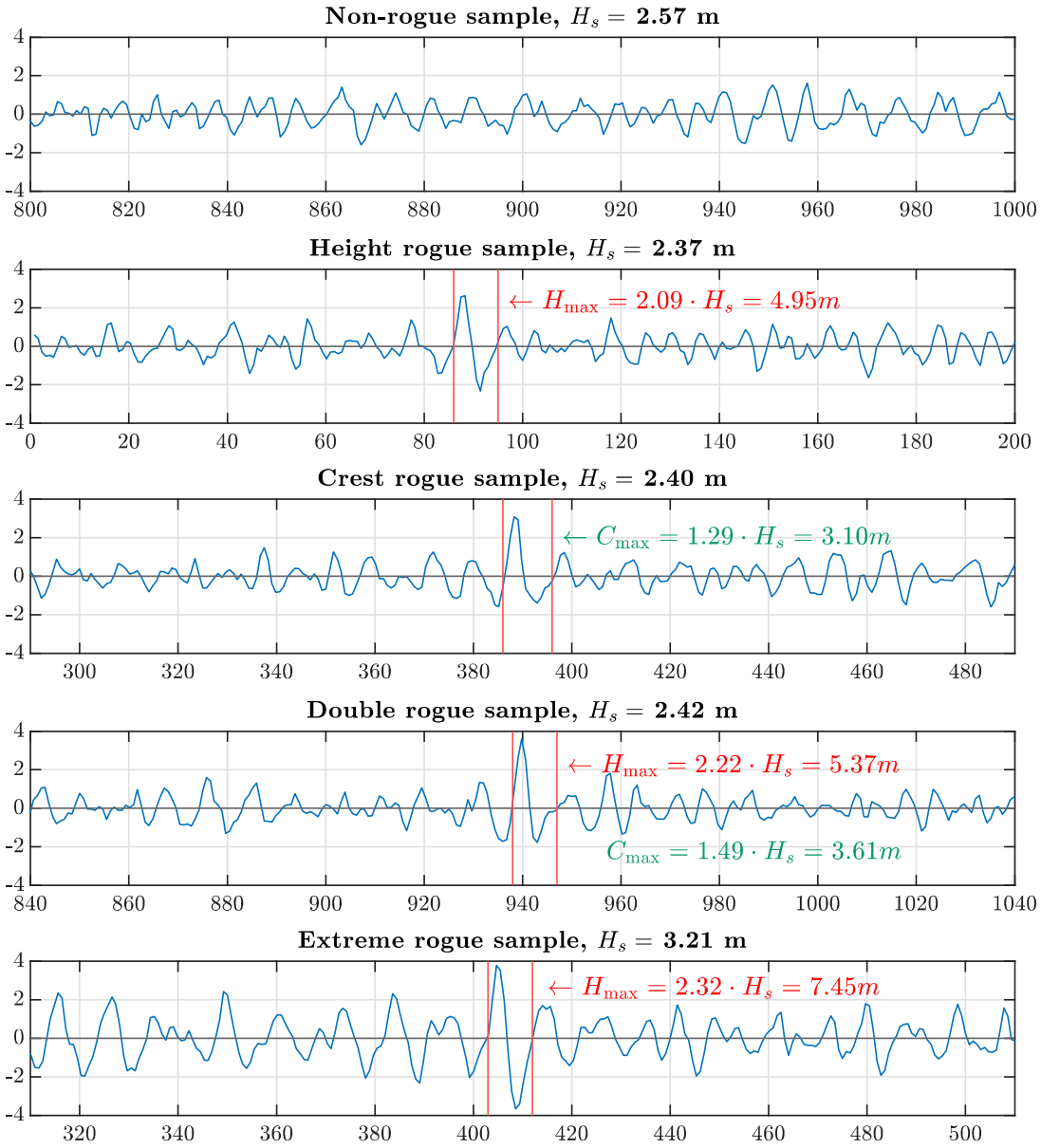

Figure 4. 200 s sections taken from example time series illustrating rogue waves for each of the four rogue wave categories, and a ~~nor-mal~~non-rogue sample with a similar value of H_s for comparison. Vertical red lines mark the two zero-upcrossings of the rogue wave. Rogue wave/crest heights are indicated in red/green.

Table 1. ~~Positions and water depths of the measurement sites.~~Number of samples and total number of individual waves in the considered time series categories.

~~Sample c~~Category	~~Normal~~Non-rogue	Height rogue	Crest rogue	Double rogue	Extreme rogue	Total
No. of samples	13,984	833	95	151	93	15,156
Total no. of waves	4,759,663	287,617	32,354	52,520	32,117	5,164,271
Sample percentage	92.3 %	5.5 %	0.6 %	1.0 %	0.6 %	100 %

2.2 Application of the Korteweg–de Vries equation with vanishing boundary conditions to the measurement data

A vKdV-NLFT was applied to the data, to obtain the discrete soliton spectrum of each time series. The KdV equation was introduced by Korteweg and de Vries (1895). It describes the evolution of weakly nonlinear and dispersive progressive unidirectional free-surface waves in shallow water ($h\ L^{-1} < 0.22$) with constant depth. For the analysis of space series (fixed at one point in time), the space-like KdV equation (sKdV) is given e.g. in Osborne (2010), with reference to Korteweg and de Vries (1895) as

$$u_t + c\ u_x + \alpha\ u\ u_x + \beta\ u_{xxx} = 0, \tag{7}$$

in which $u = u(x,t)$ is a free-surface space series, developing in space x and time t. The subscripts x and t denote partial derivatives, c is the phase speed in shallow water, $\alpha = (3c)(2h)^{-1}$ and $\beta = (ch^2)/6$ are constants, depending on the phase speed c and the water depth h. Equation (7) can be adapted to the analysis of time series (fixed at one point in space, like e.g. buoy measurements. For the case of a free-surface elevation time series $u(x_0,t)$ (see f.ex. Fig. 5) at base point x_0, it is then described by the time-like KdV equation (tKdV) (Osborne, 1993)

$$u_x + c'\ u_t + \alpha'\ u\ u_t + \beta'\ u_{ttt} = 0, \tag{8}$$

in which $c' = c^{-1} = (\sqrt{gh})^{-1}$, $\alpha' = -\alpha\ (c^2)^{-1}$ and $\beta' = -\beta\ (c^4)^{-1}$. For our application of the KdV-NLFT, we assumed initial conditions with vanishing boundaries

$$\lim_{t \to \pm\infty} u(x_0,t) = 0 \tag{9}$$

sufficiently fast. Since we were mainly interested in the soliton part of the nonlinear spectrum and solitons are not periodic, we preferred vanishing (vKdV-NLFT) to periodic (pKdV-NLFT) boundary conditions. For vanishing boundary conditions, the soliton spectrum completely describes the behaviour of the wave train in the far field (Prins and Wahls, 2019). The surface elevation in the far field is then described by

$$u(x,t) \approx \sum_{n=1}^{N} \tilde{u}_n sech^2(k_n x - \omega_n t - \phi_n), \tag{10}$$

as the linear superposition of independent solitons after the oscillatory waves have dampened out, with $\tilde{u}_n = 2k_n^2$ and $\omega_n = 4k_n^3$ (Prins and Wahls, 2019, Eq. (4), Schuur, 1984, Eq. (17), Schuur, 1986, p. 83, Eq. (3.3), Ablowitz and Kodama, 1982, Eq.

(2.20a)). In the KdV-NLFT, solitons are easily identified as the discrete part of the nonlinear spectrum. We applied the vKdV-NLFT by using the MATLAB (2019) interface to the software library FNFT (Wahls et al., 2018), development version (commit 681191c). Its solution consists of a discrete soliton spectrum and a continuous spectrum representing oscillatory waves. Figure 5 shows an example of a measurement time series ~~and its corresponding soliton spectrum.~~, its linear FFT spectrum, the nonlinear continuous spectrum and the discrete nonlinear soliton spectrum. In this paper, only the discrete soliton spectrum will be discussed further. Each of the solitons in the discrete spectrum would be a physical soliton if the signal is propagated according to the KdV equation with vanishing boundary conditions. After sufficiently long propagation, the solitons will separate and their characteristic shapes become clearly visible. For visualisation of the role of solitons in the time series, the upper plot in Fig. 5 shows the soliton train that was obtained by nonlinear superposition of the solitons (considering their interactions, but neglecting the continuous spectrum) using the algorithm from Prins and Wahls (2021). ~~Technically, the frequency axis has no physical meaning, because a soliton, for which~~Although the surface elevation composing a soliton does not cross the still water level~~, has no frequency and thus its duration should be infinitely long (Bruehl and Oumeraci (2016)). However, from the soliton solution of the tKdV, an angular frequency is obtained as~~, a mathematical definition of the angular frequency can be obtained from the soliton solution of the tKdV (Brühl et al., 2022, Eq. (12)) as

$$\Omega = 2\pi \cdot F = \sqrt{\frac{3Ag}{4h^2}}. \tag{11}$$

Since this equation relates the frequency F to the amplitude A of the soliton, the frequency sorts the solitons in the spectrum by their amplitude. ~~To distinguish them from oscillatory waves~~Following the convention in Brühl and Oumeraci (2016), the solitons in the discrete spectrum (lower panel of Fig. 5) are displayed on a negative frequency axis. The vKdV-NLFT was applied to all 15,156 samples listed in Table 1.

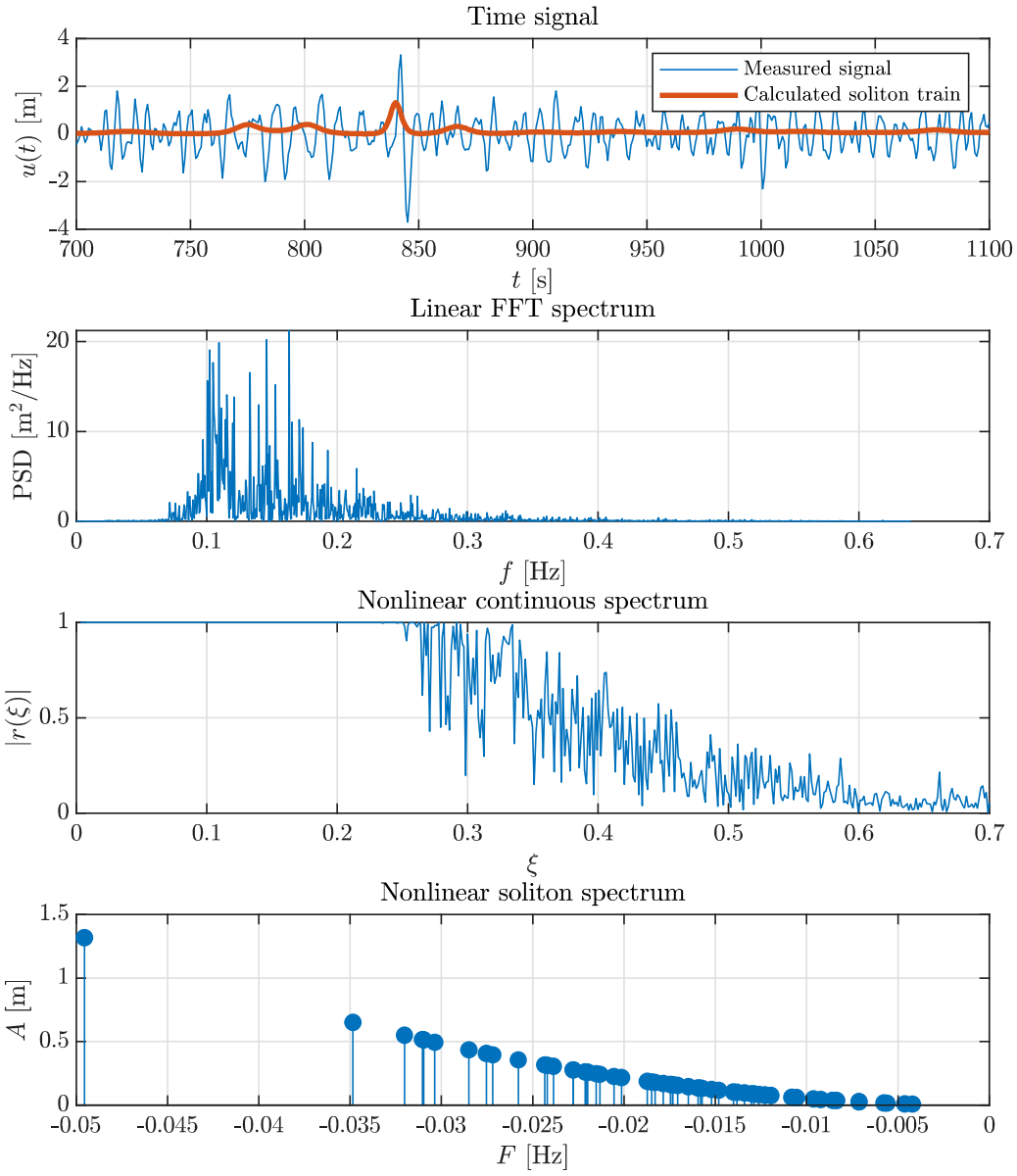

Figure 5. Example of a time series including a rogue wave at approx. 820 s, and its corresponding ~~soliton spectrum,~~FFT and NLFT spectra. The nonlinear spectra were calculated from vKdV-NLFT. The time series with $H_{\max}\, H_s^{-1} = 2.58$, $H_{\max} = 7.00$ m and $H_s = 2.71$ m, was measured on 17 October 2013, starting at 11:30. The upper panel additionally shows the soliton train, as obtained by nonlinear superposition of the solitons in the discrete spectrum (Prins and Wahls, 2021). Note that inverting large soliton spectra is numerically difficult (Prins and Wahls, 2021). Therefore, a shortened time series was used in the upper panel.

Regular and irregular wavetrains in very shallow water are known to often contain solitons, even without the presence of rogue waves (e.g., Osborne et al., 1991; Brühl and Oumeraci, 2016). The present study supports this finding: solitons ~~Solitons~~ were found in all samples, with and without rogue waves. The aim of the study was to explore the role of the ~~determined~~individual solitons for the generation of rogue waves. In the first part of the study, it was investigated whether ~~specific~~individual solitons in the NLFT spectrum could be associated with the recorded rogue waves. For this purpose, all free-surface elevations between the two zero-upcrossings of a rogue wave (or largest wave, for ~~normal~~non-rogue samples) were scaled down to 80 % (Fig. 6). The KdV-NLFT was then repeated for the modified time series, which resulted in a new soliton spectrum. It was monitored which of the solitons had changed in amplitude A (and, therefore, in frequency F), due to the change in wave height of the modified rogue wave. These solitons were assumed to have the same position in the time series as the rogue/ maximum wave. In the second part of the study, we explored whether the spectra calculated from rogue wave time series showed differences when compared to those calculated from ~~normal~~non-rogue time series.

3 Results

3.1 Attribution of solitons to rogue waves

Solitons were attributed to specific rogue waves, following the procedure described in Sect. 2.2. We found in each case that the amplitude of one large soliton significantly decreased for a reduced rogue wave (or maximum wave) height. Also in the group of smaller solitons, slight changes in amplitudes were observed. Since for solitons, amplitude A and frequency F are related according to Eq. (11), the reduction in amplitude corresponded to a simultaneous shift in frequency, which can be seen in the soliton spectrum (Fig. 6). The reduced solitons can be regarded to be associated with the rogue wave in the time series, while the other solitons in the spectrum maintained their amplitudes. The solitons with constant amplitudes can be regarded not to be associated with the rogue wave. We refer to the amplitudes of the $l = 1 \dots n$ solitons associated with the rogue wave as A_S^n, with A_S^1 denoting the largest attributed soliton. Although often the case, the largest soliton attributed to the rogue wave was not necessarily the largest soliton in the spectrum (Fig. 7).

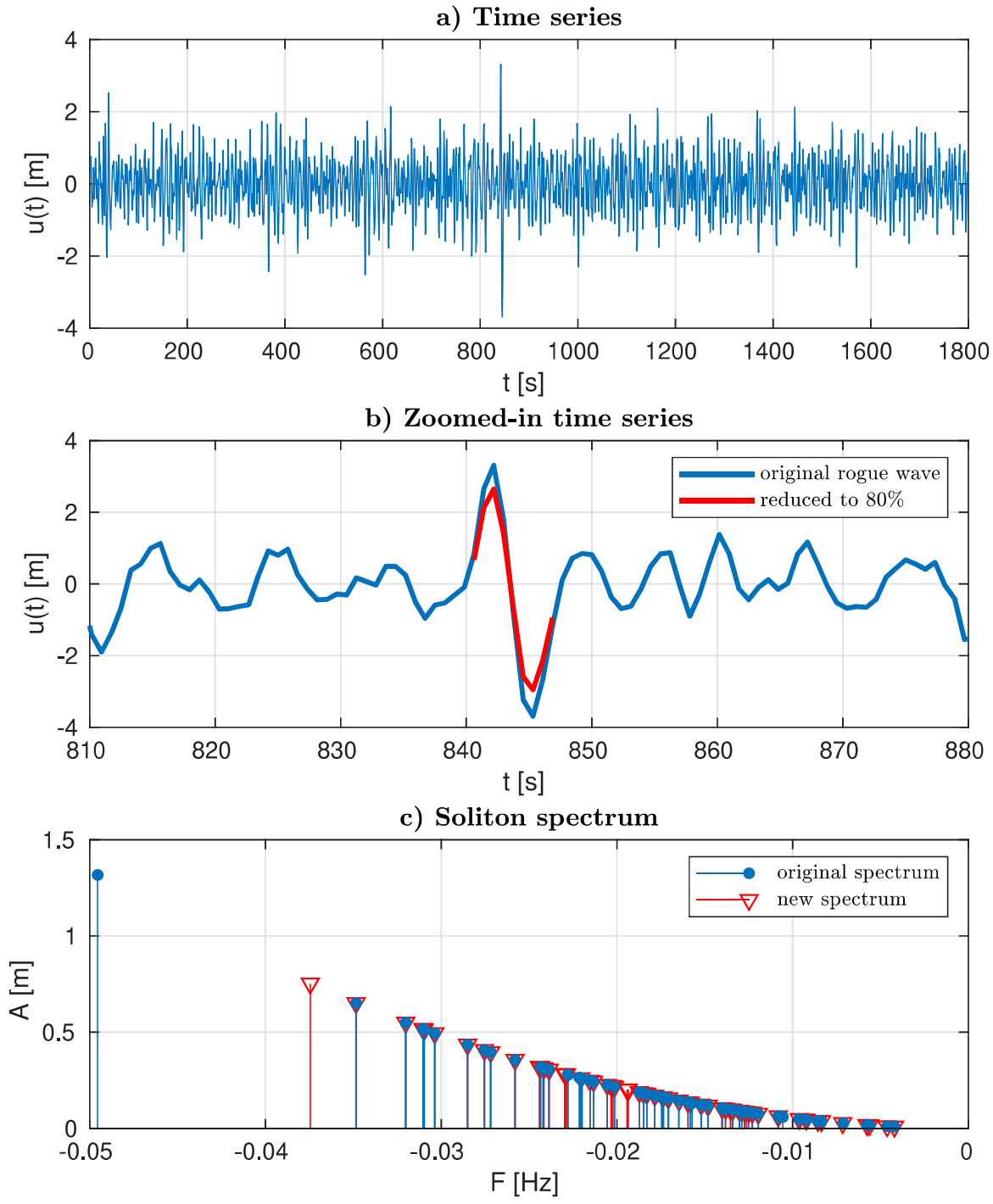

Figure 6. From top to bottom: (a) extreme rogue wave time series from 17 October 2013, starting at 11:30; (b) magnified view of the rogue wave (blue curve) and reduction of its elevation to 80 % (red curve); (c) soliton spectra of the original (blue circles) and the modified time series (red triangles), resulting from vKdV-NLFT.

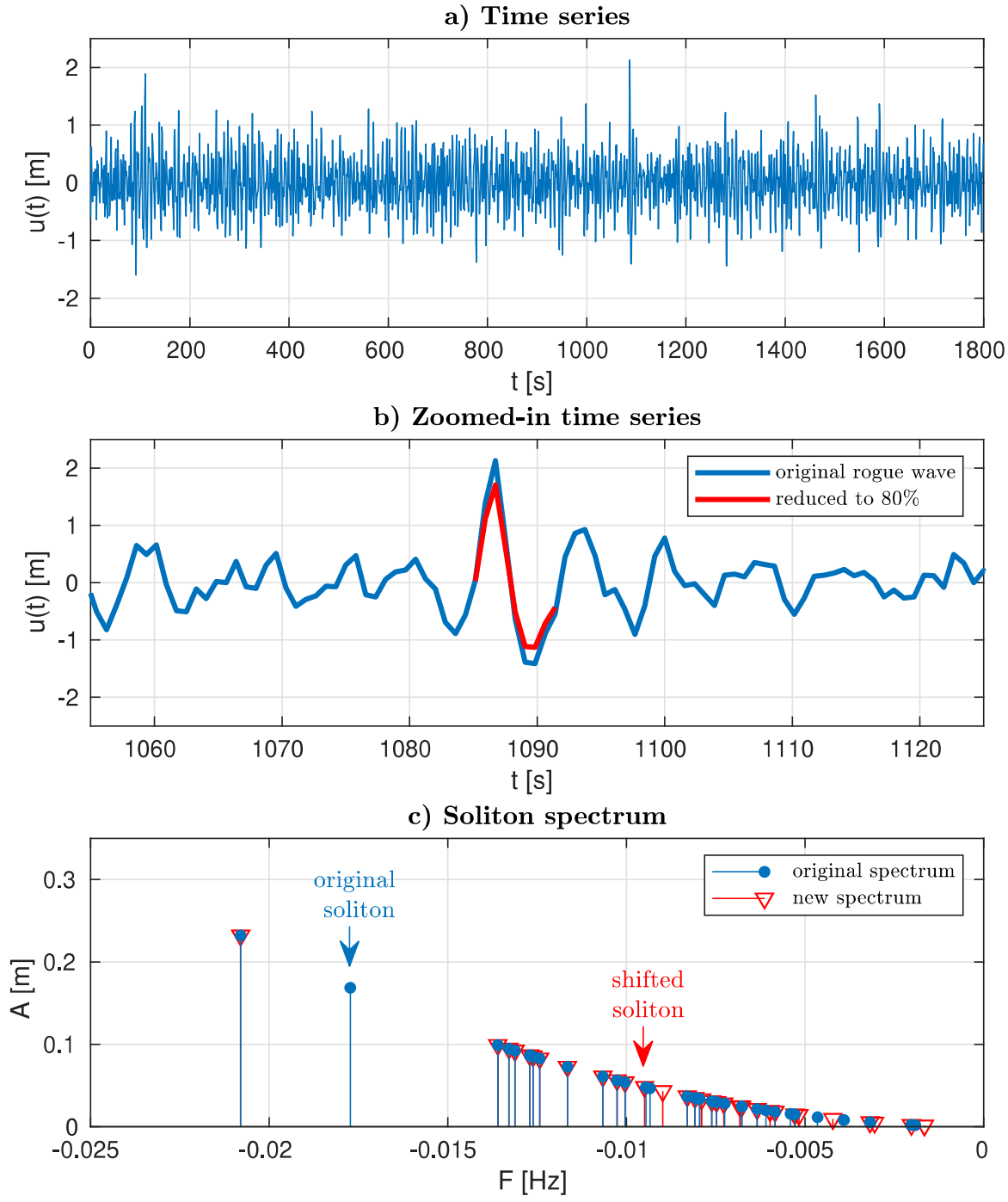

Figure 7. From top to bottom: (a) double rogue wave time series from 27 April 2016, starting at 20:30; (b) magnified view of the rogue wave (blue curve) and reduction of its elevation to 80 % (red curve); (c) soliton spectra of the original (blue circles) and the modified time series (red triangles), resulting from vKdV-NLFT.

We extracted the amplitude of the largest attributed soliton A_S^1 for each time series and compared it to the rogue wave height H (for rogue waves according to any of the two height criteria, including double rogue waves, Fig. 8(a)) or the crest height C of the rogue wave (for rogue waves according to the crest criterion, including double rogue waves, Fig. 8(b)). A comparison of the soliton amplitude A_S^1 to the largest wave height $H_{\max}$ and the largest crest height $C_{\max}$ in ~~normal~~non-rogue samples has been added for reference (Fig. 8(c) and (d)). The ~~gradients~~slopes of the linear regression curves express increasing A_S^1 with increasing H or $H_{\max}$ and C or $C_{\max}$. ~~T~~For the analysed samples, the scatter of the data suggests an upper limit of A_S^1 between 2 m and 3 m. The goodness of fit of each curve to the data is given in terms of the coefficient of determination

$$R^2 = \frac{SS_{\text{res}}}{SS_{\text{total}}}, \tag{12}$$

in which SS_{res} is the sum of squares of residuals with respect to the regression curve, and SS_{total} is the sum of squared residuals with respect to the average value of the data and thus a measure of the variance. R^2 indicates that the linear curves fit the results from height and extreme rogue wave samples better than the results from ~~normal~~non-rogue, double and crest rogue samples. R^2 is higher in Fig. 8(a) than in Fig. 8(b)-(d).

Moreover, it is seen that the amplitude of the largest soliton is always smaller than the rogue wave crest/ height itself. This is in agreement with results by Osborne et al. (1991), who identified solitons in measurement data from the Adriatic sea by applying the NLFT with quasi-periodic boundary conditions to the KdV equation. ~~Thus, the mere existence of a soliton is not sufficient to explain the presence of a rogue wave in our data.~~ Our investigation revealed that in all cases some smaller solitons were additionally associated with a rogue wave. Typical values of the amplitude of the second-largest soliton A_S^2 are 20-30 % of A_S^1. The amplitude of the third-largest attributed soliton A_S^3 is typically 10-20 % of A_S^1. ~~The interaction of unidirectional solitons, however, as described by KdV, is known not to result in exceptional increases in wave elevation (Kharif and Pelinovsky, 2003). Hence, the soliton spectrum alone does not yield a satisfactory explanation of the generation mechanism of extreme waves/ crests. One may speculate that the formation of the rogue wave in these cases is a result of the interaction of one or several solitons with the underlying oscillating wave field, a hypothesis which will need further analyses to be validated.~~

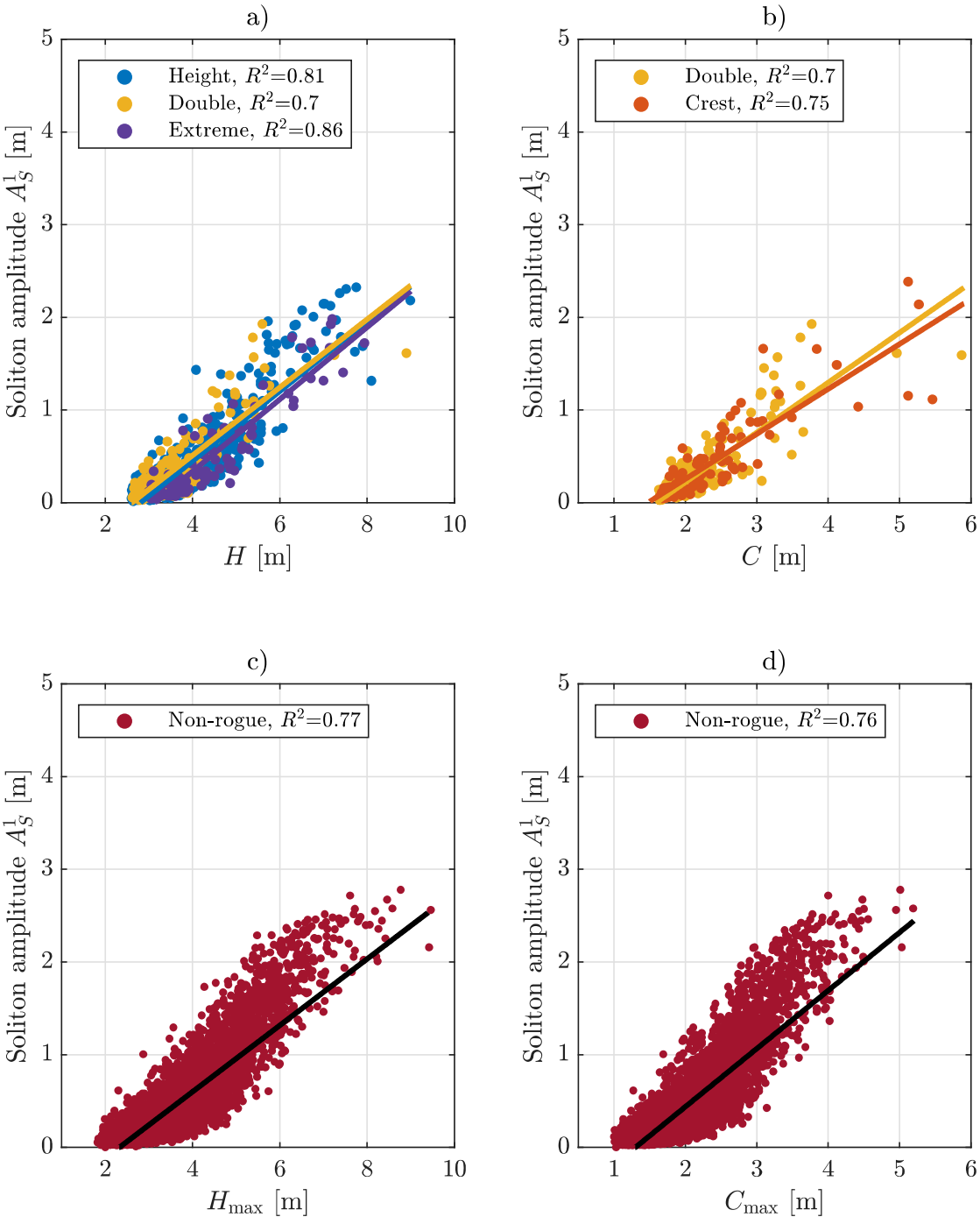

Figure 8. Amplitude of the largest soliton attributed to the highest wave, A_S^1, in the time series for ~~normal samples~~the rogue wave (upper row) or ~~the rogue wave~~non-rogue samples as a function of rogue wave height H/ maximum wave height $H_{\max}$ (left column) or rogue crest height C/ maximum crest height $C_{\max}$ (right column). The goodness of fit of the linear regression curves is given in terms of R^2.

So far, the results show that high soliton amplitudes in the spectrum are associated with high absolute values of wave heights or crests. However, this does not necessarily imply that high solitons play a role in forming individual waves that are exceptional with respect to the surrounding wave field. To ~~remove the influence of the underlying sea state~~be able to compare different measurement samples, the soliton amplitudes A_S^1 were normalised by the significant wave height H_s of the corresponding sample. By relating the normalised soliton amplitudes to the different time series categories, the importance of solitons for the relative height of rogue or maximum waves was investigated (Fig. 9). If solitons are to play a major role for the presence of rogue waves, their normalised amplitudes are expected to increase from ~~normal~~non-rogue samples with $H\ (H_s)^{-1} < 2.0$ through height and double rogue waves ($2.0 \leq H\ (H_s)^{-1} < 2.3$) to extreme rogue waves ($H\ (H_s)^{-1} \geq 2.3$). In fact, the median values of $A_S^1\ (H_s)^{-1}$ are higher for rogue wave samples than for ~~normal~~non-rogue samples, meaning the distributions calculated from the rogue wave samples are shifted ~~to the right~~towards higher normalised soliton amplitudes with respect to the distribution calculated from ~~normal~~non-rogue samples (Fig. 9). Additionally, the rogue wave sample distributions, and especially those calculated from crest and extreme rogue samples, show heavier ~~right~~ tails. The differences in the distributions suggest that solitons play a role in rogue wave generation. It is striking that not only extreme rogue waves, but also crest rogue waves had a tendency to be associated with higher solitons. This makes sense when recalling that a soliton is not an oscillating wave and because of its shape contributes more to wave crests than to wave heights. However, although differences in normalised soliton amplitudes $A_S^1\ (H_s)^{-1}$ are present for the different categories, the distributions overlap and the positive trend with increasing relative wave height is not as pronounced as the positive trend of A_S^1 with increasing maximum wave height, as presented in Fig. 8. This emphasises the relevance of the considered sea state for the soliton amplitude, in that large solitons are only found in high sea states. Large solitons correspond to high wave heights H and high crest heights C, but not necessarily to high relative wave heights $H\ (H_s)^{-1}$ or high relative crest heights $C\ (H_s)^{-1}$. ~~Consequently, the presence of a large soliton is not sufficient to explain the presence of a rogue wave. Again, it is presumed that oscillatory wave components and/ or nonlinear interactions must contribute to the formation of rogue waves.~~

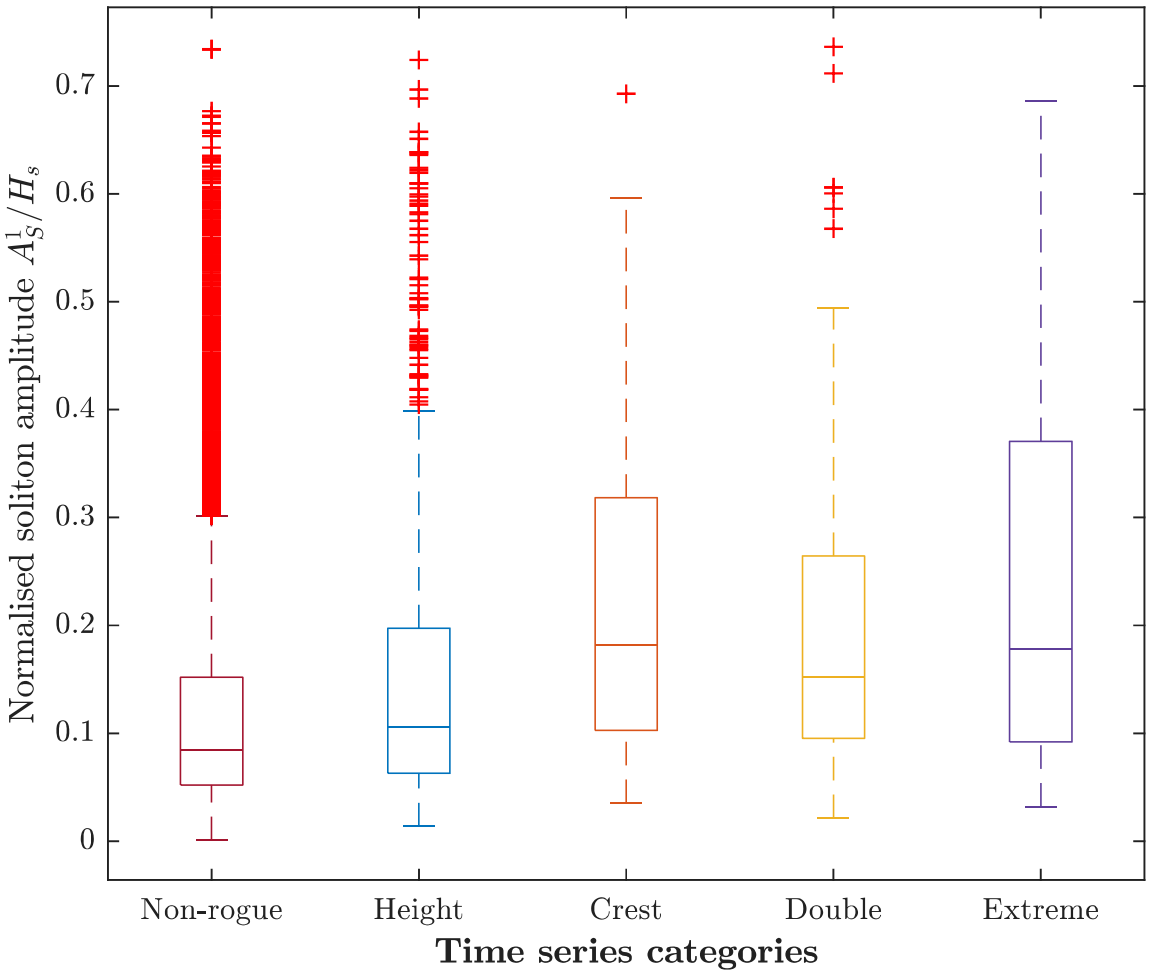

Figure 9. Amplitude of the highest soliton attributed to the rogue wave or maximum wave in the time series, normalised by the significant wave height, for the different categories of time series. Distributions are shown as box-and-whisker plots (box: interquartile range; whiskers: 1.5 times the interquartile range; horizontal line inside the box: median; red crosses: data outside the whiskers).

Since we were interested in the importance of ~~nonlinearity~~nonlinear processes in the rogue wave generation at the buoy location, we intended to quantify the nonlinearity of the rogue waves. In shallow water, the nonlinearity of waves can be described by the Ursell number (Ursell, 1953). Different definitions of the Ursell number exist. A common definition is (Dean and Dalrymple, 1991, Eq. 11.109)

$$U_1 = \frac{HL^2}{h^3} = \frac{16}{3}K^2k^2, \tag{13}$$

with K the complete elliptic integral of the first kind, and the modulus k. According to Osborne (2010, Eq. 10.151 and Eq. 10.154), the Ursell number in its time-like form is given by ~~The Ursell number in its time-like form is given, according to Osborne (2010), by~~

$$U_2 = \frac{3}{32\pi^2}\left(\frac{HL^2}{h^3}\right) = \frac{mK^2(m)}{2\pi^2}, \tag{14}$$

with the modulus m. ~~in which we interpreted $a = C$ as the maximum elevation of the rogue wave above the still water level, following LeMehaute (1976).~~ (For consistency with Eq. (13), the wave amplitude a in the original equation of Osborne (2010) has been replaced by the wave height $a = H/2$.) Comparison of Eq. (13) and Eq. (14) shows the Ursell numbers to differ by a factor of $3/(32\pi^2)$. The moduli in Eq. (13) and Eq. (14) are related by $m = k^2$. Thus, different Ursell number definitions will yield different thresholds for the separation of wave theories. In this study, we use the definition given in Eq. (14) and adjust the cited threshold values accordingly.

The Ursell number ~~U~~ is known to be an equivalent to the BFI for deep water waves (Slunyaev et al., 2011; Onorato et al., 2001) and has been used to classify wave types. ~~It has been stated that an Ursell number of $U = 0$ corresponds to linear waves, while $U = 1$ points to solitary waves (Miles, 1980).~~ In Brühl (2014), solitary-like waves are defined by a modulus of $m > 0.99$. According to this classification and by applying Eq. (14), Ursell numbers $U_2 > 0.559$ are obtained for solitary-like waves. Waves with $U_2 \leq 0.559$ are classified as oscillatory waves.

According to Eq. (14), the Ursell number is defined either by the modulus m or by height H and wavelength L of a single wave oscillation over depth h. Thus, we can calculate the Ursell number for the identified rogue waves using the H and L obtained by zero-upcrossing. In our case, the amplitudes of the largest attributed solitons show an almost linear positive trend with increasing Ursell number up until approximately $U_2 = 0.5$ (Fig. 10). ~~Brühl (2022) classifies waves with $0.559 \leq U$ as solitary-like wave types and waves with $U < 0.559$ as Airy-like, Stokes-like or cnoidal-like.~~ For our data, in which the bulk of waves are located below $U_2 = 0.559$, this means that most rogue wave ~~crests are not soliton-like~~s are not classified as solitons. This is in agreement with several previous studies, which have shown that rogue waves in shallow water, despite their large amplitudes, have very small ratios of nonlinearity to dispersion (Ursell numbers), thus are almost linear (Pelinovsky et al., 2000; Kharif and Pelinovsky, 2003; Pelinovsky and Sergeeva, 2006). ~~This again reinforces a point made earlier, that the rogue waves in our case cannot be explained by solitons alone. This may lead to the conclusion that solitons need to interact with other wave components for the formation of these rogue waves, which we have not verified.~~ Another observation made from Fig. 10 is ~~a threshold~~an upper limit in soliton amplitude between $A_S^1 = 2.0$ m and $A_S^1 = 2.8$ m, depending on the time series category, for Ursell numbers larger than approximately $U_2 = 0.5$. Referring to the classification ~~by Brühl (2022)~~given above, this implies that for the most nonlinear waves, which are those satisfying solitary wave theory, soliton amplitudes are limited. A limit in soliton height as a result of breaking is expected at amplitudes of approximately $A = 8$ m for a water depth of $h = 10$ m, as the breaking criterion for solitary waves is $A\,h^{-1} = 0.78$ (McCowan, 1891) or $A\,h^{-1} = 0.83$ (Lenau, 1966). Therefore, shallow-water wave breaking at the location of the buoy can be excluded. The reason for the limit in soliton amplitude already at $A_S^1 = 2.5$ m to $A_S^1 = 3$ m could be limited energy input by wind (see Middleton and Mellen (1985) for soliton generation by wind), or a shoal in front of the measurement buoy causing the larger waves to break before they reach the buoy.

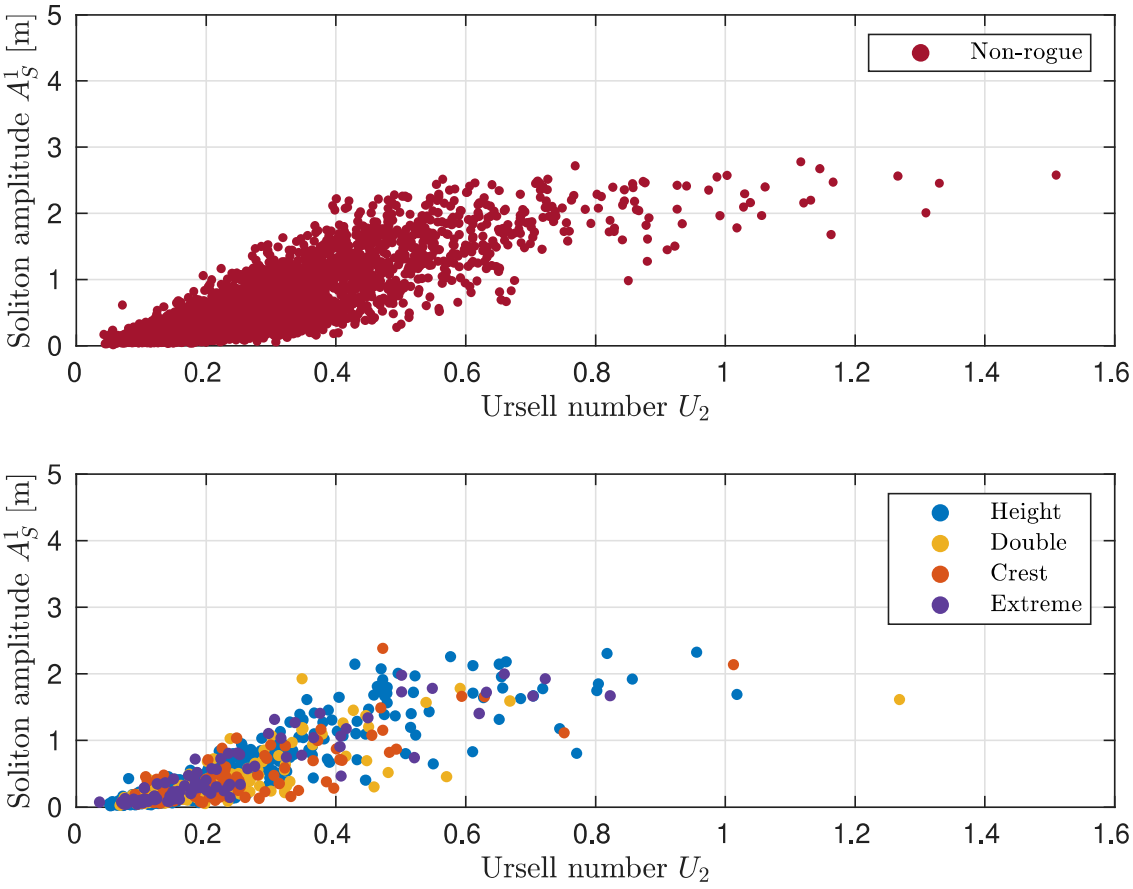

Figure 10. Upper panel: amplitude of the highest soliton attributed to the maximum wave in the time series as a function of the Ursell number of the maximum wave in the time series. Lower panel: amplitude of the highest soliton attributed to the rogue wave as a function of the Ursell number of this rogue wave.

3.2 Soliton spectra for time series with and without rogue waves

When investigating the attribution of solitons to rogue waves in Sect. 3.1, we found in the majority of cases that the largest soliton in the nonlinear spectrum could be attributed to the rogue wave. In addition, this soliton was often outstanding from the other solitons in the spectrum, with a much larger amplitude than the remaining solitons in the spectrum (see the example in Fig. 6). We were therefore interested in whether the existence of an outstanding soliton in the nonlinear spectrum was typical for rogue wave samples off Norderney. We investigated this question statistically by comparing soliton spectra, calculated from vKdV-NLFT, for ~~normal~~non-rogue samples and the four different categories of rogue wave samples. In fact, while all 15.156 considered time series yielded discrete spectra with a large number of solitons, we identified two characteristic classes of

soliton spectra. The typical appearance of a soliton spectrum calculated from a time series without rogue waves, was a cluster of solitons (Fig. 11). On the contrary, soliton spectra calculated from time series including a rogue wave in the majority of cases showed one outstanding soliton with an amplitude much larger than that of the remaining cluster of solitons in the spectrum (Fig. 5).

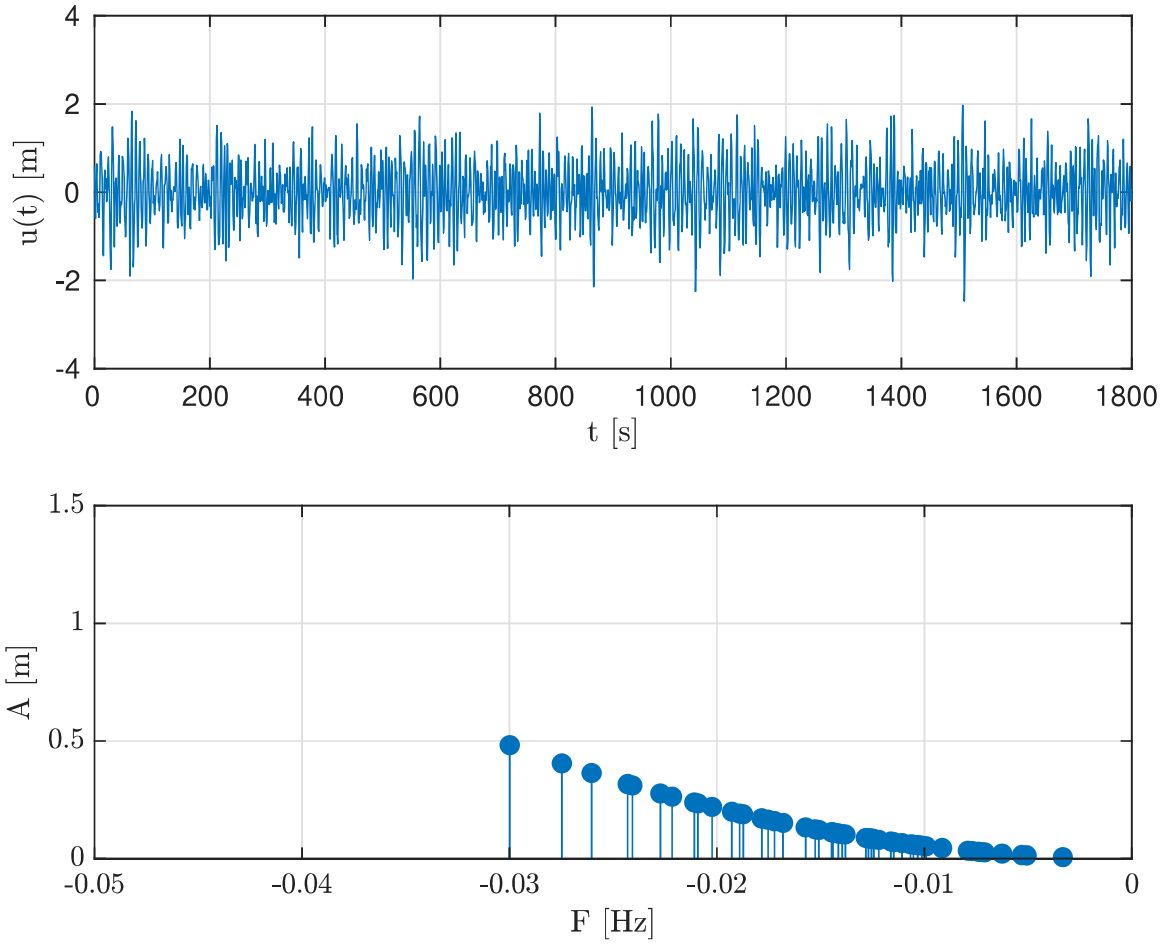

Figure 11. Example of a ~~normal~~non-rogue time series without rogue waves, and its corresponding soliton spectrum, calculated from vKdV-NLFT. The soliton spectrum displays a cluster of solitons, found to be typical for the majority of spectra calculated from ~~normal~~non-rogue time series. The time series was measured on 26 December 2016, starting at 11:30, with the parameters $H_{\max} = 4.44$ m, $H_s = 2.46$ m and $H_{\max}\,(H_s)^{-1} = 1.80$.

To distinguish between clustered soliton spectra and those featuring an outstanding soliton, we compared the amplitudes of the largest soliton, A_1, and the second-largest soliton, A_2, in the discrete spectrum. From the visual inspection of the spectra,

we identified a threshold of the ratio $A_2\ (A_1)^{-1}$, below which the largest soliton could be called outstanding:

$$\frac{A_2}{A_1} \leq 0.8. \tag{15}$$

Thus, a soliton spectrum had an outstanding soliton if the second-largest soliton was at least 20 $\%$ smaller than the largest soliton in the spectrum. The choice of this threshold was further supported by the fact that the threshold $A2\ (A1)^{-1} = 0.8$ coincides with the median value of $A2\ (A1)^{-1}$ for maximum wave heights just below the rogue wave criterion $H\ (H_s)^{-1} \geq 2.0$ (Fig. 12). This reveals that our threshold chosen for the distinction between clustered spectra and those featuring an outstanding soliton, at the same time indicates a difference between the spectra calculated from ~~normal~~non-rogue and those calculated from rogue wave time series.

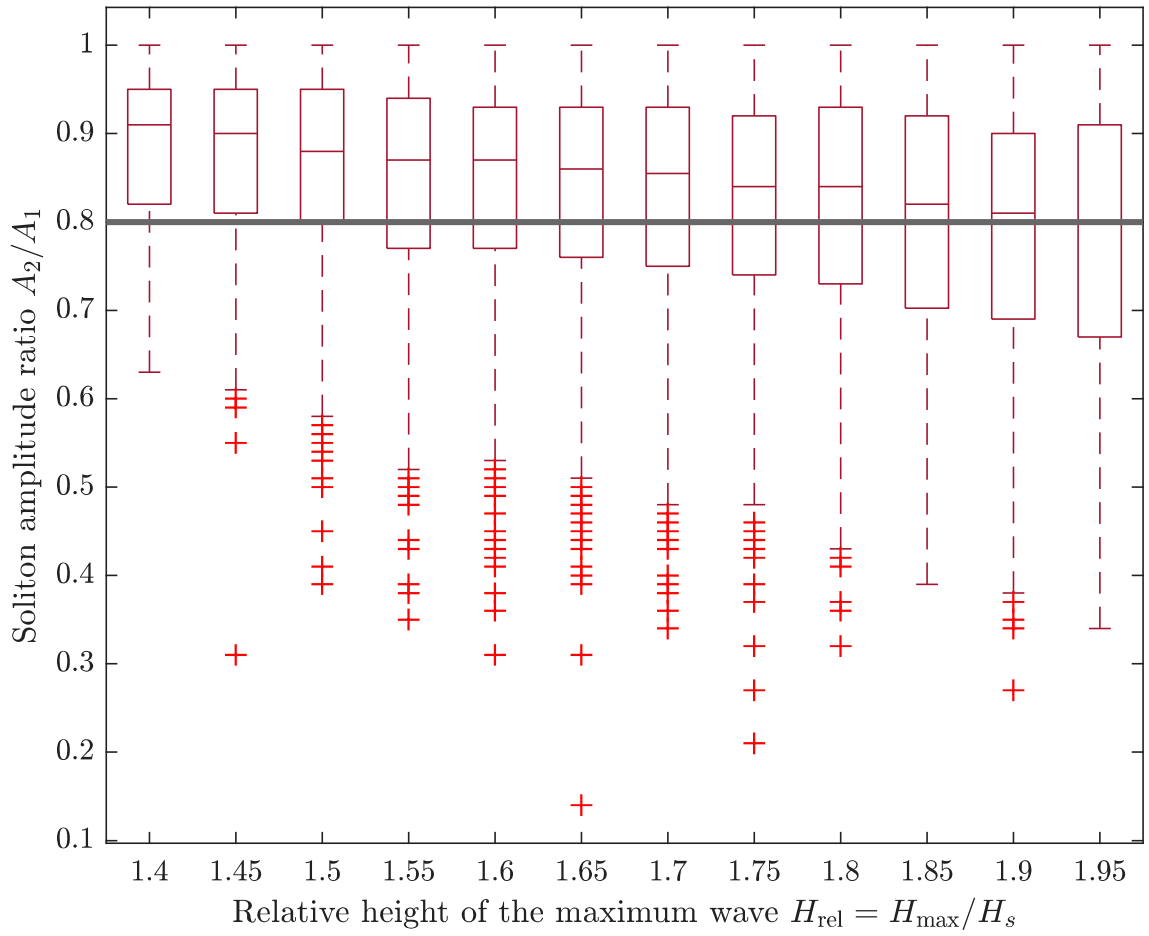

Figure 12. Distribution of the ratio between the second-largest and the largest soliton in the discrete spectrum calculated from ~~normal~~non-rogue time series. $H\ (H_s)^{-1}$ bins of width 0.05 are shown up until $H\ (H_s)^{-1} < 2.0$, which corresponds to the definition of height rogue waves (Eq. (4)). Distributions are shown as box-and-whisker plots (box: interquartile range; whiskers: 1.5 times the interquartile range; horizontal line inside the box: median; red crosses: data outside the whiskers).

Equation (15) is valid for 30 minute samples at the measurement site, which is the standard window size of measurement samples delivered by Datawell Waverider buoys. Since the ratio between soliton amplitudes might be dependent on the window size, it is not clear if Eq. (15) would apply to other than 30 minute time windows. The effect of a larger time window size will be discussed in Sect. 4. Table 2 shows the share of outstanding solitons and clustered soliton spectra in each of the categories defined in Sect. 2.1. It is seen that the typical appearance of the soliton spectrum for 30 minute wave measurement samples off Norderney without rogue waves is a cluster of solitons (64 % of the samples), while at the same time it is not unlikely to obtain a soliton spectrum with one outstanding soliton from vKdV-NLFT (36 % of the samples). For 30 minute rogue wave samples

in contrast, it is more likely to obtain a soliton spectrum with one outstanding soliton than a clustered soliton spectrum. This is true for height rogue samples (57 %), and even more pronounced for crest rogue samples (64 %), double rogue samples (72 %) and, finally, extreme rogue samples (87 %). The conclusion can be drawn that the absence of an outstanding soliton is a strong ~~predictor~~indicator for the absence of an extreme rogue wave. The differences between the four rogue wave categories, indicating that the presence of an outstanding soliton is not equally expressive for all types of rogue waves, may lead to the presumption that not all rogue waves found off Norderney can necessarily be explained by the same theory.

Table 2. Share of samples in each category showing an outstanding soliton or a clustered soliton spectrum, respectively.

	~~Normal~~Non-rogue	Height rogue	Crest rogue	Double rogue	Extreme rogue
Outstanding soliton	36 %	57 %	64 %	72 %	87 %
Clustered solitons	64 %	43 %	36 %	28 %	13 %

The question whether inferences can be made from the time to the spectral domain and vice versa, is answered by a contingency table (Fig. 13). Here, all previously defined rogue wave categories are combined into one joint group of rogue wave samples. Two statements can be made based on the table. On the one hand, the probability that an NLFT spectrum calculated from a normal sample shows an outstanding soliton, is 4986/13.984 = 36 %, while the probability that a spectrum calculated from a rogue wave sample shows an outstanding soliton, is 726/1172 = 62 %. This indicates that, although not all rogue waves can necessarily be explained by the same theory, outstanding solitons occurred in connection with the majority of observed rogue waves off Norderney. While in the combined group of rogue waves, outstanding solitons play a role in 62 % of the cases, the share differs between the rogue wave categories (Table 2). On the other hand, although rogue waves are more likely to be observed when an outstanding soliton is present in the NLFT spectrum, the presence of an outstanding soliton alone is not sufficient as an indicator for the detection of rogue waves. The main difficulty is the imbalance in sample size between ~~normal samples~~non-rogue and rogue wave samples.

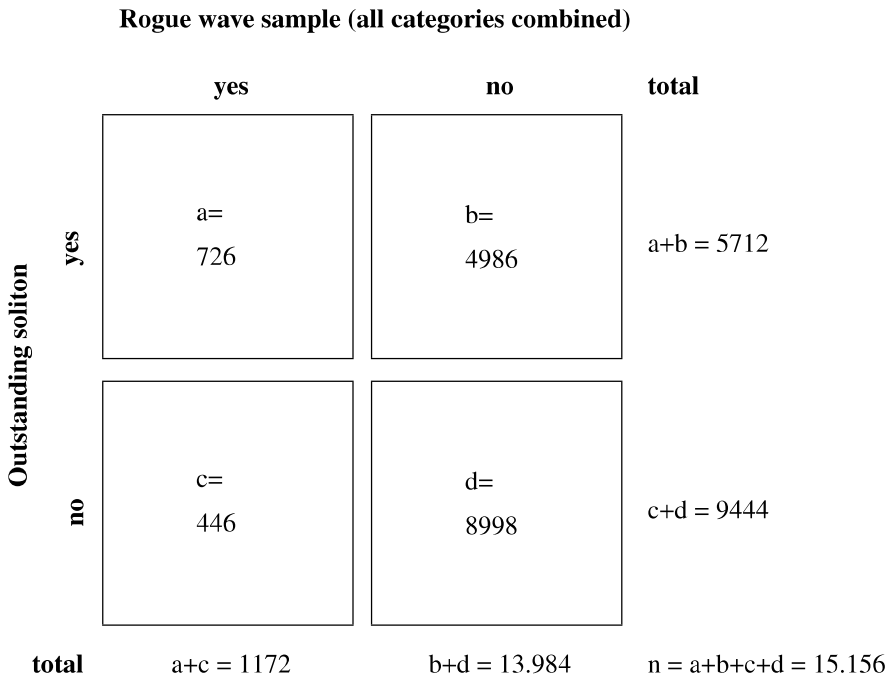

Figure 13. Contingency table of forecast/event pairs. a- hits. b- false alarms. c- misses. d- correct negatives.

In Fig. 14, the ratio between the amplitudes of the second-largest and the largest soliton in the nonlinear spectrum, $A_2\,(A_1)^{-1}$, is visualised in a boxplot for each of the time series categories. A ratio above $A_2\,(A_1)^{-1} = 0.8$, meaning that the second-largest soliton has a rather similar amplitude to the largest soliton, implies that the soliton spectrum is clustered (Eq. (15)). For ~~nor-mal~~non-rogue samples, this is the case for the bulk of time series. The median of the ratio $A_2\,(A_1)^{-1}$ decreases from the most-left to the most-right category on the right axes in Fig. 14. For height rogue waves, the median of $A_2\,(A_1)^{-1}$ is below the 80 %-line, with the distribution extending above and below. For double and extreme rogue waves, the gap between the soliton amplitudes may become much larger than for height rogue waves. In some cases, the amplitude A_2 amounts to less than 30 % of the amplitude A_1. In all categories except extreme rogue samples, there are samples for which the first and second solitons are almost similar in amplitude ($A_2\,(A_1)^{-1} \approx 1$). On the contrary, for all extreme rogue wave samples, A_2 is below 93 % of A_1. The large part of soliton spectra from extreme rogue samples shows an outstanding soliton.

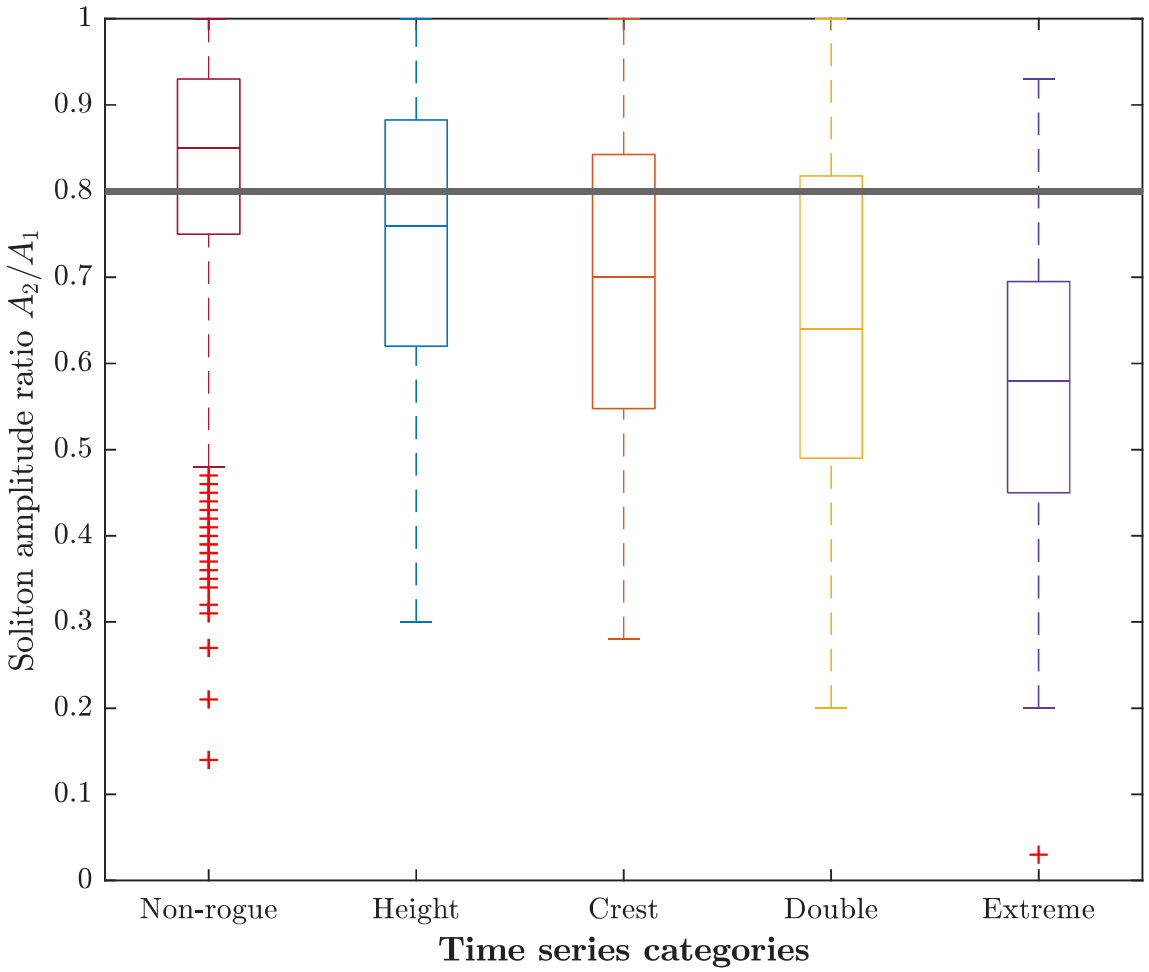

Figure 14. Boxplots of the ratio between the second-largest soliton (A_2) and the largest soliton (A_1) in the spectrum for the different categories of time series. Distributions are shown as box-and-whisker plots (box: interquartile range; whiskers: 1.5 times the interquartile range; horizontal line inside the box: median; red crosses: data outside the whiskers). Below the horizontal line of 80 %, the highest soliton in the spectrum is classified as outstanding.

Figure 15 presents the ratio $A_2\ (A_1)^{-1}$ in a scatter plot with one data point for each individual time series. According to this representation, although the presence of an outstanding soliton with $A_2\ (A_1)^{-1} \leq 0.8$ is not a useful indicator of whether a rogue wave is present in the time series or not, the presence of a rogue wave becomes much more likely when one soliton in the nonlinear spectrum is strongly outstanding with $A_2\ (A_1)^{-1} \leq 0.3$: of all 23 samples satisfying $A_2\ (A_1)^{-1} \leq 0.3$, only $4/23 = 17$ % are ~~normal~~non-rogue samples, while $19/23 = 83$ % of the samples are rogue wave samples (1 height, 1 crest, 8 double, 9 extreme rogue wave samples).

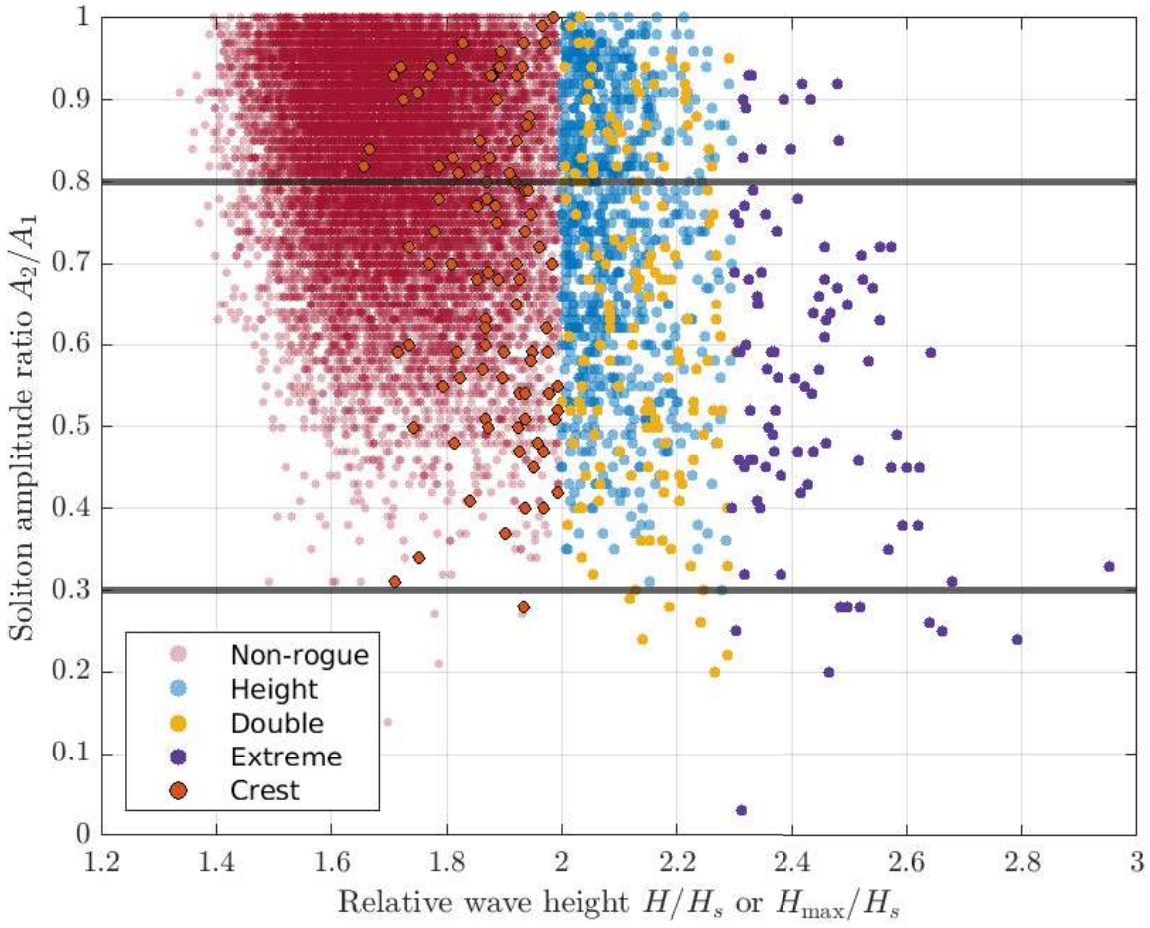

Figure 15. Ratio between the second-largest soliton (A_2) and the largest soliton (A_1) in the spectrum as a function of relative wave height $H\ (H_s)^{-1}$ or $H_{\max}\ (H_s)^{-1}$ for the different categories of time series. Below the horizontal line of 80 %, the highest soliton in the spectrum is classified as outstanding. Below the horizontal line of 30 %, the highest soliton in the spectrum is referred to as strongly outstanding.

4 Discussion

We investigated discrete nonlinear soliton spectra obtained by the application of the vKdV-NLFT to time series measured by a surface-following buoy off the coast of the island Norderney in the southern North Sea. The impulse for investigating the data at this specific site by using nonlinear methods was given by a previous study (Teutsch et al., 2020). There, it was found that while ~~second-order distributions were~~the Forristall distribution was sufficient to describe rogue wave occurrences at nearby buoy stations in somewhat deeper water (see kh ranges of buoy stations in Table 1 of Teutsch et al. (2020)), the Norderney buoy recorded a larger number of rogue waves than expected according to ~~second-order theory~~the Forristall distribution. The results

described in this paper suggest that nonlinear processes may explain the enhanced rogue wave occurrence at this specific site. The results were derived by the application of vKdV-NLFT and are therefore strictly valid for shallow-water conditions in the context of the applicability of the KdV equation. In a future study, it may be interesting to extend the investigation to additional ~~shallow-water~~ sites in shallow water depths.

Throughout the study, indications were found that although solitons play a role for the presence of rogue waves at Norderney, the soliton spectrum alone does not yield a satisfactory explanation of the formation of extreme waves/ crests. A first hint is given in the upper panel of Fig. 5, which shows the reconstructed soliton train along with the measured time series. Here, solitons (and their interactions) neither account for the full height of the observed rogue wave nor provide the observed wave trough. Fig. 8 supports the finding that the solitons were not large enough to explain the full heights of the associated rogue waves. From Fig. 9, it is seen that the presence of a large soliton is not necessarily connected to the presence of a rogue wave. Another indication that the soliton spectrum alone is not sufficient to explain the presence of rogue waves is given in Fig. 10, which shows that the shapes of most rogue wave crests are not soliton-like. In addition, Kharif and Pelinovsky (2003) found that the interaction of unidirectional KdV solitons does not result in exceptional increases in wave elevation. As a consequence, one may speculate that the formation of the rogue waves in our data set was a result of nonlinear interactions of one or more solitons with the underlying oscillating wave field. This hypothesis will need further analyses to be validated.

The bathymetry below the measurement buoy at Norderney is characterized by a strong decrease in water depth. Non-Gaussian wave characteristics as a result of decreasing water depth have already been described e.g. by Huntley et al. (1977)~~,~~ in the context of wave run-up. It has ~~and~~ gained increased attention in the context of rogue wave occurrence (e.g., Sergeeva et al., 2011). Increased rogue wave frequencies behind slopes or steps were confirmed by numerous numerical (e.g., Sergeeva et al., 2011; Majda et al., 2019) and experimental studies (e.g., Trulsen et al., 2012; Kashima et al., 2014; Ma et al., 2014; Zhang et al., 2019; Trulsen et al., 2020)(Raustøl, 2014; Jorde, 2018; Bolles et al., 2019; Zhou et al., 2019). ~~Li et al. (2021) have explained the higher occurrence of rogue waves due to an abrupt depth transition from deeper to shallower water by additional second-order free waves generated at the transition.~~The main subject that the mentioned studies are concerned with~~,~~ is that waves propagating over a slope, step or bar, are forced into new equilibrium conditions (Zeng and Trulsen, 2012). This mechanism is associated with strong non-Gaussian statistics and an increased rogue wave probability (Zhang and Benoit, 2021). The reason for the enhanced rogue wave probability was identified as the higher degree of nonlinearity in the shallow water behind the slope or step, which leads to an enhancement of second-order harmonic bound waves (Gramstad et al., 2013). Zheng et al. (2020) and Li et al. (2021) confirmed numerically and theoretically that second-order terms (made up from bound waves and free waves released by the interaction of bound waves with the slope) are responsible for peaks in skewness and kurtosis. Zhang and Benoit (2021) stated that both second- and third-order effects evolving from the non-equilibrium dynamics at the depth transition significantly enhance the local kurtosis and the occurrence of rogue waves. For these effects to occur, the shallow domain must be sufficiently shallow and the slope of the bathymetry change plays a major role (Fu et al., 2021). The largest peaks in kurtosis and skewness and the highest rogue wave probabilities were found for the steepest slopes (Gramstad et al., 2013; Zheng et al., 2020; Fu et al., 2021; Lawrence et al., 2021). Doeleman (2021) recently showed in tank experiments that the findings are not valid in shallow water. Mendes et al. (2022) confirmed theoretically that a strong amplification may be found in intermediate water

($0.5 < kh < 1.5$). They stated that "Whether rogue waves are enhanced in strong bathymetry changes throughout most oceans or regionally under suitable conditions is yet to be assessed" (Mendes et al., 2022). Zeng and Trulsen (2012) anticipate that ~~it~~the described mechanisms may explain the spatially varying occurrence frequency of rogue waves on the continental shelf, where waves enter from the deep sea. Therefore, the described processes associated with a strong decrease in depth might be an explanation for the observed increased rogue wave occurrence off the coast of Norderney (Teutsch et al., 2020). A connection between rogue waves and solitons in this context was established by Sergeeva et al. (2011). The authors showed by applying a KdV equation, that the number of solitons increases in the shallow water behind a slope. They linked this increased soliton occurrence to an increased rogue wave probability.

The solutions of the KdV equation for a given free-surface elevation time series strongly depend on the water depth (see Eq. (7)). While for our calculations, we assumed a constant water depth of $h = 10$ m, there are in fact major uncertainties regarding the water depth at the actual location of the buoy, due to tidal changes and bathymetry gradients, together with the movement of the buoy, as mentioned in Sect. 2.1 (Fig. 2). The mean tidal range at Norderney is approximately ~~± 1.25 m~~2.5 m, while due to an additional movement of the buoy of 2 m to each side of the slope a total deviation from the nominal water depth of ± 2 m is reasonable. We performed a sensitivity analysis to test the robustness of the results with respect to these uncertainties. To do so, we repeated the computation of the soliton spectrum for water depths of $h = 8$ m and 12 m, respectively, while using the same free-surface data as in the previous analysis. A changed water depth leads to a different ~~shallow-water conditions~~depth range in which the KdV equation is valid (Eq. (3)). For the calculation with a depth of $h = 12$ m, we repeated the identification of the samples that fulfill shallow-water conditions in the KdV context, as samples and maximum waves due to the larger water depth now had to satisfy the condition T_p or $T > 5$ s, in order to classify as shallow~~-water~~depth samples/ waves for the applicability of the KdV equation. Therefore, only 14.206 samples, that is, approximately 94 % of the original sample size, were available for the calculation at $h = 12$ m. For the calculation with a depth of $h = 8$ m, we used the same samples as for the calculation with $h = 10$ m, because these automatically fulfilled shallow~~-water~~ depth conditions at $h = 8$ m. Irrespective of the water depth adopted in the calculation, the result remained that samples with rogue waves, and especially extreme rogue waves, were more likely to contain an outstanding soliton in the nonlinear spectrum than samples without rogue waves (Table 3). Thus, the results are robust with respect to potential uncertainties in water depth.

Table 3. Share of samples in each category showing an outstanding soliton in the soliton spectrum, for the respective water depth adopted in the NLFT calculation. Note that for a water depth of $h = 12$ m, the shallow~~-water~~-depth criterion in Eq. (3) changes to $T_p > 5$ s, which left approximately 94 % of the samples for the calculation at a water depth of 12 m.

Water depth	~~Normal~~Non-rogue	Height rogue	Crest rogue	Double rogue	Extreme rogue
8 m	32 %	57 %	61 %	73 %	75 %
10 m	36 %	57 %	64 %	72 %	87 %
12 m	36 %	53 %	62 %	70 %	76 %

The KdV equation is only valid for unidirectional waves. Although Osborne (1993) recommends the application of the NLFT for KdV to measurement data only for samples in which the largest part of the energy is in the dominant propagation direction, we applied the KdV-NLFT outside the limits that are given in the literature. At our measurement site, the sea state was always multidirectional, with a directional spreading of the wave energy approximately between 28° and 55°, while in the dataset of Osborne (1993), only 5 % of the energy were perpendicular to the dominant direction of propagation. We repeated the first part of the analysis, for which the results are described in Sect. 3.1, for the approximately 10 % of samples in each category with the lowest directional spread. This corresponded to a threshold in directional spread of 35° for most categories, except crest rogue waves, which tended to occur in broader sea states (threshold at 36.5°) and extreme rogue waves, which statistically occur in more narrow sea states (Christou and Ewans, 2014) (threshold at 34°). We found our result- that an outstanding soliton is more typical for a rogue wave time series than for a ~~normal~~non-rogue time series- confirmed and partly emphasised (Table 4). Therefore, we rate vKdV-NLFT, although assuming unidirectionality in multidirectional measurement samples, an appropriate tool to evaluate the connection between solitons and rogue waves off Norderney.

Table 4. Share of samples in each category showing an outstanding soliton, for the approximately 10 % most narrow samples.

	~~Normal~~Non-rogue	Height rogue	Crest rogue	Double rogue	Extreme rogue
No. of samples	1614	91	12	17	10
Outstanding soliton	31 %	57 %	67 %	88 %	90 %

In our study, we have applied the vKdV-NLFT as a trace method for (extreme) rogue waves and demonstrated for the first time that certain distinctive patterns in the NLFT spectrum of real-world time series indicate extreme rogue waves. The method may provide further information on possibly dangerous time series in future applications. Further research is required on the applicability of the KdV equation to our data, which cannot be validated on the basis of single-point measurements. If wave propagation at Norderney is well described by KdV theory, the NLFT spectrum is approximately constant during propagation. The method may then identify time series with the potential of forming extreme rogue waves. Moreover, even if the KdV equation does not describe the propagation well, we still consider the NLFT a more appropriate transform than the linear FFT, which is often applied even if waves are nonlinear. Similar to the FFT in the linear case, our method should be treated as a signal transform (Sugavanam et al., 2019). Our study provides insights into the spectral characteristics at the considered site.

We would like to put an emphasis on the limitation of our suggested definition of an outstanding soliton (Eq. (15)) to the size of the measurement window. Our criterion was chosen based on the inspection of soliton spectra from 30 minute time series. However, the gap size might change depending on the chosen window size. An increase in window size, meaning more waves in the time series, will introduce additional solitons to the spectrum. If these are larger than A_1 or emerge in between A_1 and A_2, the gap size between the two largest solitons will be influenced. If these are smaller than A_2, their emergence will not alter the gap between A_1 and A_2. Similarly, a reduction in window size would exclude waves in the time series and remove solitons corresponding to these waves. If this modification leads to the removal of the largest or second-largest soliton, the gap

between the new A_1 and A_2 will become larger or smaller than for a 30 minute time window. If this modification only affects solitons smaller than A_2, the size of the gap between A_1 and A_2 will not be influenced. We applied the ratio between A_2 and A_1 merely as a measure to statistically evaluate differences in the soliton spectra calculated from 30 minute ~~normal~~non-rogue and rogue wave time series. For different window sizes, it might be necessary to define new criteria.

Due to the limited recording frequency of the wave buoy, one might question the correct assignment of time series to the different categories (Table 1). Wave crests might be missed by the discrete measurement points, leading to a possible underestimation of rogue or extreme rogue waves (Stansell et al., 2002). However, even if extreme rogue time series were assigned incorrectly to the category of height rogue waves, this misinterpretation is conservative: none of the time series in the category "extreme rogue samples" has been assigned incorrectly. Furthermore, according to the sampling theorem (Shannon, 1949), the buoy sampling rate of 1.28 Hz is sufficient to sample time series whose FFT spectra decay at approximately 0.6 Hz (Fig. 5, second panel). Therefore, we consider the buoy sampling frequency sufficient for our purpose.

Our result that rogue wave samples have a higher probability of showing an outstanding soliton in the nonlinear spectrum compared to ~~normal~~non-rogue samples becomes most obvious in the categories of double and extreme rogue samples. In these categories, differences from ~~normal~~non-rogue samples are visible not only in the percentage of outstanding solitons, but also in the magnitude of the amplitude gap between the first and second solitons in the spectrum. Height rogue waves, on the contrary, do not seem to differ very much from high waves in ~~normal~~non-rogue samples, both in terms of the gap between first and second soliton in the spectrum, and the height of the solitons associated with the maximum wave. The fact that differences between time series with and without rogue waves become apparent only in some of the chosen categories, raises the question whether the choice of rogue wave definitions has been reasonable for the considered location. The rogue wave definitions serving as a basis to this study have been introduced by Haver and Andersen (2000) for deep water waves. The relative height and crest values in their definitions represent outliers, being exceeded in 1 of 100 cases when applying a second-order model to the deep-water sea-surface elevation (Haver, 2000). The definitions have been taken up numerous times in the literature. Authors have been investigating whether rogue waves according to Haver and Andersen's definition (2000) are outliers with respect to typical wave distributions in the real ocean as well (e.g., Forristall, 2005; Gemmrich and Garrett, 2008). The question has been raised whether the rogue wave definition by a certain height or crest threshold is useful in practice (Häfner et al., 2021). Several authors have, based on large measurement datasets, come to the conclusion that these rogue waves are rare, but nevertheless realisations of commonly used wave distributions (e.g., Waseda et al., 2011; Christou and Ewans, 2014). In a previous study (Teutsch et al., 2020), we were able to confirm this conclusion at buoy measurement stations in intermediate water. However, at the ~~shallow water~~ buoy station off Norderney in comparably shallow water depth, which showed a larger number of rogue waves than expected according to the common wave distributions, the interaction of solitons with oscillating waves might be a mechanism explaining the increased occurrence of rogue waves.

5 Conclusions

Rogue wave occurrence recorded off the coast of the island Norderney is not sufficiently explained by ~~second-order theory~~the Forristall distribution of wave heights. We investigated the role of solitons as components of the discrete vKdV-NLFT spectrum in the enhanced rogue wave occurrence ~~by calculating discrete soliton spectra of time series from vKdV-NLFT~~. Our main results for this specific measurement site are the following.

- Each measured rogue wave could be associated with at least one soliton in the NLFT spectrum.
- The soliton heights were always smaller than those of the rogue waves. Samples with rogue waves were more likely to contain an outstanding soliton in the NLFT spectrum than samples without rogue waves.
- The soliton spectrum analysis is a good indicator of extreme rogue waves in the corresponding time series.
- The presence of a strongly outstanding soliton, with a ratio between the second-largest and the largest soliton in the nonlinear spectrum of $A_2\ (A_1)^{-1} \leq 0.3$, was found to be a strong indicator for the presence of a rogue wave.
- Conversely, the absence of an outstanding soliton in the spectrum is a strong indicator for the absence of an extreme rogue wave of $H\ (H_s)^{-1} \geq 2.3$.

We conclude that nonlinear processes are important in the generation of rogue waves at this specific site and may explain the enhanced occurrence of such waves beyond ~~second-order theory~~common wave height distributions. Rogue waves at Norderney are likely to be a result of the interaction of solitons with the underlying field of oscillatory waves. The nature of this interaction should be subject to further research.

Author contributions. All authors contributed to the idea and scope of the paper. IT performed the analyses and wrote the manuscript. MB, RW and SW provided help with data analysis, discussed the results, and contributed to the writing of the paper. RW supervised the work.

Competing interests. The authors declare that they have no conflict of interest.

Acknowledgements. Ina Teutsch received funding for this work from the Federal Maritime and Hydrographic Agency (BSH). Sander Wahls and Markus Brühl received funding from the European Research Council (ERC) under the European Union's Horizon 2020 research and innovation programme (grant agreement No 716669). The buoy data were kindly provided by the Lower Saxony Water Management, Coastal Defence and Nature Conservation Agency (NLWKN).

References

Ablowitz, M. J., Kaup, D. J., Newell, A. C., and Segur, H.: The Inverse Scattering Transform-Fourier Analysis for Nonlinear Problems, Studies in Applied Mathematics, 53, 249–315, https://doi.org/10.1002/sapm1974534249, 1974.

Alber, I. E.: The effects of randomness on the stability of two-dimensional surface wavetrains, Proceedings of the Royal Society of London. A. Mathematical and Physical Sciences, 363, 525–546, https://doi.org/10.1098/rspa.1978.0181, 1978.

Baschek, B. and Imai, J.: Rogue Wave Observations Off the US West Coast, Oceanography, 24, 158–165, https://doi.org/10.5670/oceanog.2011.35, 2011.

Benjamin, T. B. and Feir, J. E.: The disintegration of wave trains on deep water, Journal of Fluid Mechanics, 27, 417–430, https://doi.org/10.1017/s002211206700045x, 1967.

Bitner, E. M.: Non-linear effects of the statistical model of shallow-water wind waves, Applied Ocean Research, 2, 63–73, https://doi.org/10.1016/0141-1187(80)90031-0, 1980.

Brühl, M. and Oumeraci, H.: Analysis of long-period cosine-wave dispersion in very shallow water using nonlinear Fourier transform based on KdV equation, Applied Ocean Research, 61, 81–91, https://doi.org/10.1016/j.apor.2016.09.009, 2016.

Cattrell, A. D., Srokosz, M., Moat, B. I., and Marsh, R.: Can Rogue Waves Be Predicted Using Characteristic Wave Parameters?, Journal of Geophysical Research: Oceans, 123, 5624–5636, https://doi.org/10.1029/2018jc013958, 2018.

Christou, M. and Ewans, K.: Field Measurements of Rogue Water Waves, Journal of Physical Oceanography, 44, 2317–2335, https://doi.org/10.1175/jpo-d-13-0199.1, 2014.

Clamond, D., Francius, M., Grue, J., and Kharif, C.: Long time interaction of envelope solitons and freak wave formations, European Journal of Mechanics - B/Fluids, 25, 536–553, https://doi.org/10.1016/j.euromechflu.2006.02.007, 2006.

de León, S. P. and Soares, C. G.: Hindcast of extreme sea states in North Atlantic extratropical storms, Ocean Dynamics, 65, 241–254, https://doi.org/10.1007/s10236-014-0794-6, 2014.

Dysthe, K., Krogstad, H. E., and Müller, P.: Oceanic Rogue Waves, Annual Review of Fluid Mechanics, 40, 287–310, https://doi.org/10.1146/annurev.fluid.40.111406.102203, 2008.

Dysthe, K. B. and Trulsen, K.: Note on Breather Type Solutions of the NLS as Models for Freak-Waves, Physica Scripta, T82, 48, https://doi.org/10.1238/physica.topical.082a00048, 1999.

Fedele, F., Herterich, J., Tayfun, A., and Dias, F.: Large nearshore storm waves off the Irish coast, Scientific Reports, 9, https://doi.org/10.1038/s41598-019-51706-8, 2019.

Fernandez, L., Onorato, M., Monbaliu, J., and Toffoli, A.: Modulational instability and wave amplification in finite water depth, Natural Hazards and Earth System Sciences, 14, 705–711, https://doi.org/10.5194/nhess-14-705-2014, 2014.

Forristall, G. Z.: On the statistical distribution of wave heights in a storm, Journal of Geophysical Research, 83, 2353, https://doi.org/10.1029/jc083ic05p02353, 1978.

Forristall, G. Z.: Understanding rogue waves: Are new physics really necessary?, 2005.

Gardner, C. S., Greene, J. M., Kruskal, M. D., and Miura, R. M.: Method for solving the Korteweg–deVries equation., Phys. Rev. Lett., 19: 1095-7(Nov. 6, 1967)., https://doi.org/10.1103/PhysRevLett.19.1095, 1967.

Garett, C. and Gemmrich, J.: Rogue waves, Physics Today, 62, 62–63, https://doi.org/10.1063/1.3156339, 2009.

Gemmrich, J. and Garrett, C.: Unexpected Waves, Journal of Physical Oceanography, 38, 2330–2336, https://doi.org/10.1175/2008jpo3960.1, 2008.

Gramstad, O. and Trulsen, K.: Influence of crest and group length on the occurrence of freak waves, Journal of Fluid Mechanics, 582, 463–472, https://doi.org/10.1017/s0022112007006507, 2007.

Häfner, D., Gemmrich, J., and Jochum, M.: Real-world rogue wave probabilities, Scientific Reports, 11, https://doi.org/10.1038/s41598-021-89359-1, 2021.

Hammack, J., Scheffner, N., and Segur, H.: Two-dimensional periodic waves in shallow water, Journal of Fluid Mechanics, 209, 567–589, https://doi.org/10.1017/s0022112089003228, 1989.

Haver, S.: Evidences of the existence of freak waves, in: Proc. Rogue Waves, Brest, 2000.

Haver, S. and Andersen, O. J.: Freak waves: rare realizations of a typical population or typical realizations of a rare population?, in: The Tenth International Offshore and Polar Engineering Conference, International Society of Offshore and Polar Engineers, 2000.

Huntley, D. A., Guza, R. T., and Bowen, A. J.: A universal form for shoreline run-up spectra?, Journal of Geophysical Research, 82, 2577–2581, https://doi.org/10.1029/jc082i018p02577, 1977.

Janssen, P. A. E. M.: Nonlinear Four-Wave Interactions and Freak Waves, Journal of Physical Oceanography, 33, 863–884, 2003.

Janssen, P. A. E. M. and Onorato, M.: The Intermediate Water Depth Limit of the Zakharov Equation and Consequences for Wave Prediction, Journal of Physical Oceanography, 37, 2389–2400, https://doi.org/10.1175/jpo3128.1, 2007.

Johnson, D.: DIWASP, a directional wave spectra toolbox for MATLAB®: User Manual, Centre for Water Research, University of Western Australia., 2002.

Karmpadakis, I., Swan, C., and Christou, M.: Laboratory investigation of crest height statistics in intermediate water depths, Proceedings of the Royal Society A: Mathematical, Physical and Engineering Sciences, 475, 20190 183, https://doi.org/10.1098/rspa.2019.0183, 2019.

Karmpadakis, I., Swan, C., and Christou, M.: Assessment of wave height distributions using an extensive field database, Coastal Engineering, 157, 103 630, https://doi.org/10.1016/j.coastaleng.2019.103630, 2020.

Kashima, H., Hirayama, K., and Mori, N.: ESTIMATION OF FREAK WAVE OCCURRENCE FROM DEEP TO SHALLOW WATER REGIONS, Coastal Engineering Proceedings, 1, 36, https://doi.org/10.9753/icce.v34.waves.36, 2014.

Kharif, C. and Pelinovsky, E.: Physical mechanisms of the rogue wave phenomenon, European Journal of Mechanics - B/Fluids, 22, 603–634, https://doi.org/10.1016/j.euromechflu.2003.09.002, 2003.

Korteweg, D. J. and de Vries, G.: XLI. On the change of form of long waves advancing in a rectangular canal, and on a new type of long stationary waves, The London, Edinburgh, and Dublin Philosophical Magazine and Journal of Science, 39, 422–443, https://doi.org/10.1080/14786449508620739, 1895.

Lenau, C. W.: The solitary wave of maximum amplitude, Journal of Fluid Mechanics, 26, 309–320, https://doi.org/10.1017/s0022112066001253, 1966.

Longuet-Higgins, M. S.: On the Statistical Distribution of the Height of Sea Waves, Journal of Marine Research, 11, 1952.

Ma, Y., Dong, G., and Ma, X.: EXPERIMENTAL STUDY OF STATISTICS OF RANDOM WAVES PROPAGATING OVER A BAR, Coastal Engineering Proceedings, 1, 30, https://doi.org/10.9753/icce.v34.waves.30, 2014.

Majda, A. J., Moore, M. N. J., and Qi, D.: Statistical dynamical model to predict extreme events and anomalous features in shallow water waves with abrupt depth change, Proceedings of the National Academy of Sciences, 116, 3982–3987, https://doi.org/10.1073/pnas.1820467116, 2019.

MATLAB: version 9.6.0.1072779 (R2019a), The MathWorks Inc., Natick, Massachusetts, 2019.

McCowan, J.: VII. On the solitary wave, The London, Edinburgh, and Dublin Philosophical Magazine and Journal of Science, 32, 45–58, https://doi.org/10.1080/14786449108621390, 1891.

Middleton, D. and Mellen, R.: Wind-generated solitons: A potentially significant mechanism in ocean surface wave generation and surface scattering, IEEE Journal of Oceanic Engineering, 10, 471–476, https://doi.org/10.1109/JOE.1985.1145130, 1985.

NLWKN: Tideaußenpegel, https://www.pegelonline.nlwkn.niedersachsen.de/Pegel/TideauÃ§enpegel/ID/452, accessed: 2021-12-23, 2021.

Olagnon, M. and v. Iseghem, S.: Some observed characteristics of sea states with extreme waves, in: Proc. 10th Int. Offshore Polar Engineering Conf., Seattle, pp. 84–90, International Society of Offshore and Polar Engineers, 2000.

Onorato, M., Osborne, A. R., Serio, M., and Bertone, S.: Freak Waves in Random Oceanic Sea States, Physical Review Letters, 86, 5831–5834, https://doi.org/10.1103/physrevlett.86.5831, 2001.

Orzech, M. D. and Wang, D.: Measured Rogue Waves and Their Environment, Journal of Marine Science and Engineering, 8, 890, https://doi.org/10.3390/jmse8110890, 2020.

Osborne, A. R.: Behavior of solitons in random-function solutions of the periodic Korteweg–de Vries equation, Physical Review Letters, 71, 3115–3118, https://doi.org/10.1103/physrevlett.71.3115, 1993.

Osborne, A. R.: Nonlinear ocean waves and the inverse scattering transform, Elsevier, Amsterdam, 2010.

Osborne, A. R., Segre, E., Boffetta, G., and Cavaleri, L.: Soliton basis states in shallow-water ocean surface waves, Physical Review Letters, 67, 592–595, https://doi.org/10.1103/physrevlett.67.592, 1991.

Pelinovsky, E. and Sergeeva, A.: Numerical modeling of the KdV random wave field, European Journal of Mechanics - B/Fluids, 25, 425–434, https://doi.org/10.1016/j.euromechflu.2005.11.001, 2006.

Pelinovsky, E., Talipova, T., and Kharif, C.: Nonlinear-dispersive mechanism of the freak wave formation in shallow water, Physica D: Nonlinear Phenomena, 147, 83–94, https://doi.org/10.1016/s0167-2789(00)00149-4, 2000.

Peregrine, D. H.: Water waves, nonlinear Schrödinger equations and their solutions, The Journal of the Australian Mathematical Society. Series B. Applied Mathematics, 25, 16–43, https://doi.org/10.1017/S0334270000003891, 1983.

Peterson, P., Soomere, T., Engelbrecht, J., and van Groesen, E.: Soliton interaction as a possible model for extreme waves in shallow water, Nonlinear Processes in Geophysics, 10, 503–510, https://doi.org/10.5194/npg-10-503-2003, 2003.

Pinho, U., Liu, P., Eduardo, C., and Ribeiro, C.: Freak Waves at Campos Basin, Brazil, Geofizika, 21, 2004.

Prevosto, M.: Effect of Directional Spreading and Spectral Bandwidth on the Nonlinearity of the Irregular Waves, 1998.

Sergeeva, A., Pelinovsky, E., and Talipova, T.: Nonlinear random wave field in shallow water: variable Korteweg-de Vries framework, Natural Hazards and Earth System Sciences, 11, 323–330, https://doi.org/10.5194/nhess-11-323-2011, 2011.

Serio, M., Onorato, M., Osborne, A., and Janssen, P.: On the computation of the Benjamin-Feir Index, Il Nuovo Cimento C, 28, 893–903, https://doi.org/10.1393/ncc/i2005-10134-1, 2006.

Shrira, V. I. and Geogjaev, V. V.: What makes the Peregrine soliton so special as a prototype of freak waves?, Journal of Engineering Mathematics, 67, 11–22, https://doi.org/10.1007/s10665-009-9347-2, 2010.

Slunyaev, A., Didenkulova, I., and Pelinovsky, E.: Rogue waters, Contemporary Physics, 52, 571–590, https://doi.org/10.1080/00107514.2011.613256, 2011.

Slunyaev, A., Sergeeva, A., and Didenkulova, I.: Rogue events in spatiotemporal numerical simulations of unidirectional waves in basins of different depth, Natural Hazards, 84, 549–565, https://doi.org/10.1007/s11069-016-2430-x, 2016.

Slunyaev, A. V.: A high-order nonlinear envelope equation for gravity waves in finite-depth water, Journal of Experimental and Theoretical Physics, 101, 926–941, https://doi.org/10.1134/1.2149072, 2005.

Slunyaev, A. V. and Shrira, V. I.: On the highest non-breaking wave in a group: fully nonlinear water wave breathers versus weakly nonlinear theory, Journal of Fluid Mechanics, 735, 203–248, https://doi.org/10.1017/jfm.2013.498, 2013.

Soares, C. G., Cherneva, Z., and Antão, E.: Characteristics of abnormal waves in North Sea storm sea states, Applied Ocean Research, 25, 337–344, https://doi.org/10.1016/j.apor.2004.02.005, 2003.

Soomere, T.: Rogue waves in shallow water, The European Physical Journal Special Topics, 185, 81–96, https://doi.org/10.1140/epjst/e2010-01240-1, 2010.

Soomere, T. and Engelbrecht, J.: Interaction of shallow-water solitons as a possible model for freak waves, 2005.

Stansell, P.: Distributions of freak wave heights measured in the North Sea, Applied Ocean Research, 26, 35–48, https://doi.org/10.1016/j.apor.2004.01.004, 2004.

Tayfun, M. A.: Distributions of Envelope and Phase in Wind Waves, Journal of Physical Oceanography, 38, 2784–2800, https://doi.org/10.1175/2008jpo4008.1, 2008.

Teutsch, I., Weisse, R., Moeller, J., and Krueger, O.: A statistical analysis of rogue waves in the southern North Sea, Natural Hazards and Earth System Sciences, 20, 2665–2680, https://doi.org/10.5194/nhess-20-2665-2020, 2020.

Toffoli, A., Fernandez, L., Monbaliu, J., Benoit, M., Gagnaire-Renou, E., Lefèvre, J. M., Cavaleri, L., Proment, D., Pakozdi, C., Stansberg, C. T., Waseda, T., and Onorato, M.: Experimental evidence of the modulation of a plane wave to oblique perturbations and generation of rogue waves in finite water depth, Physics of Fluids, 25, 091 701, https://doi.org/10.1063/1.4821810, 2013.

Trulsen, K., Zeng, H., and Gramstad, O.: Laboratory evidence of freak waves provoked by non-uniform bathymetry, Physics of Fluids, 24, 097 101, https://doi.org/10.1063/1.4748346, 2012.

Trulsen, K., Raustøl, A., Jorde, S., and Rye, L. B.: Extreme wave statistics of long-crested irregular waves over a shoal, Journal of Fluid Mechanics, 882, R2, https://doi.org/10.1017/jfm.2019.861, 2020.

Ursell, F.: The long-wave paradox in the theory of gravity waves, Mathematical Proceedings of the Cambridge Philosophical Society, 49, 685–694, https://doi.org/10.1017/s0305004100028887, 1953.

Wahls, S. and Poor, H. V.: Fast Numerical Nonlinear Fourier Transforms, IEEE Transactions on Information Theory, 61, 6957–6974, https://doi.org/10.1109/tit.2015.2485944, 2015.

Wahls, S., Chimmalgi, S., and Prins, P. J.: FNFT: A Software Library for Computing Nonlinear Fourier Transforms, Journal of Open Source Software, 3, 597, https://doi.org/10.21105/joss.00597, 2018.

Waseda, T., Hallerstig, M., Ozaki, K., and Tomita, H.: Enhanced freak wave occurrence with narrow directional spectrum in the North Sea, Geophysical Research Letters, 38, n/a–n/a, https://doi.org/10.1029/2011gl047779, 2011.

Zakharov, V. E. and Shabat, A. B.: A scheme for integrating the nonlinear equations of mathematical physics by the method of the inverse scattering problem. I, Functional Analysis and Its Applications, 8, 226–235, https://doi.org/10.1007/bf01075696, 1975.

Zeng, H. and Trulsen, K.: Evolution of skewness and kurtosis of weakly nonlinear unidirectional waves over a sloping bottom, Natural Hazards and Earth System Sciences, 12, 631–638, https://doi.org/10.5194/nhess-12-631-2012, 2012.

Zhang, J. and Benoit, M.: Wave–bottom interaction and extreme wave statistics due to shoaling and de-shoaling of irregular long-crested wave trains over steep seabed changes, Journal of Fluid Mechanics, 912, https://doi.org/10.1017/jfm.2020.1125, 2021.

Zhang, J., Benoit, M., Kimmoun, O., Chabchoub, A., and Hsu, H.-C.: Statistics of Extreme Waves in Coastal Waters: Large Scale Experiments and Advanced Numerical Simulations, Fluids, 4, 99, https://doi.org/10.3390/fluids4020099, 2019.

Ablowitz, M. J. and Kodama, Y.: Note on Asymptotic Solutions of the Korteweg-de Vries Equation with Solitons, Studies in Applied Mathematics, 66(2), pp. 159-170, 1982.

Ablowitz, M. J. and Segur, H.: Solitons and the Inverse Scattering Transform, Philadelphia: SIAM, 1981.

Bolles, C., Speer, K., and Moore, M.: Anomalous wave statistics induced by abrupt depth change, Physical Review Fluids 4, 2019.

Brühl, M.: Direct and inverse nonlinear Fourier transform based on the Korteweg-de Vries equation (KdV-NLFT) - A spectral analysis of nonlinear surface waves in shallow water, PhD thesis, TU Braunschweig, Germany, URL http://www.digibib.tu-bs.de/?docid=00058144, 2014.

Brühl, M., Prins, P. J., Ujvary, S., Barranco, I., Wahls, S., and Liu, P. L.-F.: Comparative analysis of bore propagation over long distances using conventional linear and KdV-based nonlinear Fourier transform, Wave Motion, Volume 111, 102905, 2022.

Casas-Prat, M., Holthuijsen, L., and van Gelder, P. H. A. J. M.: Short-term statistics of 10,000,000 waves observed by buoys, Proceedings of the Coastal Engineering Conference, 560-572, 2009.

Costa, A., Osborne, A.R., Resio, D.T., Alessio, S., Chrivi, E., Saggese, E., Bellomo, K., and Long, C.K.: Soliton Turbulence in Shallow Water Ocean Surface Waves, Phys. Rev. Lett. 113, 108501, 2014.

Dean, R. and Dalrymple, R.: Water wave mechanics for engineers and scientists, World Scientific, 1984.

Didenkulova, E.: Catalogue of rogue waves occurred in the World Ocean from 2011 to 2018 reported by mass media sources, Ocean and Coastal Management, 188, 105 076, https://doi.org/10.1016/j.ocecoaman.2019.105076, 2020

Didenkulova, I.I., Nikolkina, I.F., and Pelinovsky, E.N.: Rogue waves in the basin of intermediate depth and the possibility of their formation due to the modulational instability, JETP letters 97, 194-198, 2013.

Dingemans, M.W.: Water Wave Propagation Over Uneven Bottoms, World Scientific, 1997.

Doeleman, M.W.: Rogue waves in the Dutch North Sea, Master thesis, TU Delft, 2021.

Fedele, F., Brennan, J., De Leon, S., Dudley, J., and Dias, F.: Real world ocean rogue waves explained without the modulational instability, Sci. Rep. 6, 27715, 2016.

Fu, R., Ma, Y., Dong, G., and Perlin, M.: A wavelet-based wave group detector and predictor of extreme events over unidirectional sloping bathymetry, Ocean Eng. 229, 2021.

Giovanangeli, J.-P., Kharif, C., and Stepanyants, Y.A.: Soliton spectra of random water waves in shallow basins, Math. Model. Nat. Phenom., 13, 40, 2018.

Glukhovskiy, B.: Investigation of sea wind waves (in russian), Gidrometeoizdat, 1966.

Gramstad, O., Zeng, H., Trulsen, K., and Pedersen, G.: Freak waves in weakly nonlinear unidirectional wave trains over a sloping bottom in shallow water, Physics of Fluids 25, 2013.

Hammack, J. L. and Segur, H.: The Korteweg-de Vries equation and water waves. Part 2. Comparison with experiments, Journal of Fluid Mechanics, 65(2), pp. 289-314, 1974.

Jorde, S.: Kinematiken i bölger over en grunne, Master thesis, University of Oslo, 2018.

Lawrence, C., Trulsen, K., and Gramstad, O.: Statistical properties of wave kinematics in long-crested irregular waves propagating over non-uniform bathymetry, Physics of Fluids, 33, 2021.

Li, Y., Draycott, S., Zheng, Y., Lin, Z., Adcock, T. A., and van den Bremer, T. S.: Why rogue waves occur atop abrupt depth transitions, Journal of Fluid Mechanics, 919, R5, https://doi.org/10.1017/jfm.2021.409, 2021.

Massel, S.: Ocean surface waves: Their physics and prediction, 3rd ed., World Scientific, Singapore, 2017.

Mendes, S. and Scotti, A.: The Rayleigh-Haring-Tayfun distribution of wave heights in deep water, Applied Ocean Research 113, 102739, 2021.

Mendes, S., Scotti, A., Brunetti, M., and Kasparian, J.: Non-homogeneous analysis of rogue wave probability evolution over a shoal, Journal of Fluid Mechanics, 939, DOI:10.1017/jfm.2022.206, 2022.

Onorato, M., Cavaleri, L., Randoux, S., et al.: Observation of a giant nonlinear wave-packet on the surface of the ocean, Sci. Rep., 11, 23606, 2021.

Osborne, A. R. and Bergamasco, L.: The solitons of Zabusky and Kruskal revisited: Perspective in terms of the periodic spectral transform, Physica D: Nonlinear Phenomena, 18(1-3), pp. 26-46, 1986.

Osborne, A. R.: The inverse scattering transform: Tools for the nonlinear Fourier analysis and filtering of ocean surface waves, Chaos Solitons Fractals, 5(12), pp. 2623-2637, 1995.

Osborne, A.R., Resio, D.T., Costa, A., et al.: Highly nonlinear wind waves in Currituck Sound: dense breather turbulence in random ocean waves, Ocean Dynamics 69, 187-219, 2019.

Osborne, A. R. and Petti, M.: Laboratory-generated, shallow-water surface waves: Analysis using the periodic, inverse scattering transform, Phys. Fluids, 6(5), pp. 1727-1744, 1994.

Prins, P. J. and Wahls, S.: Soliton Phase Shift Calculation for the Korteweg-De Vries Equation, IEEE Access, Volume 7, pp. 122914-122930, 2019.

Prins, P. J. and Wahls, S.: An accurate O(N2) floating point algorithm for the Crum transform of the KdV equation, Communications in Nonlinear Science and Numerical Simulation, Volume 102, p. 105782, 2021.

Raustöl, A.: Freake bölger over variabelt dyp (in Norwegian), Master thesis, University of Oslo, 2014.

Schuur, P.: Multisoliton phase shifts in the case of a nonzero reflection coefficient, Phys. Lett. A, 102(9), pp. 387-392, 1984.

Schuur, P. C.: Asymptotic Analysis of Soliton Problems: An Inverse Scattering Approach, 1232 ed. (Lecture Notes in Mathematics): A. Dold and B. Eckmann, Eds. New York, NY, USA: Springer-Verlag, 1986.

Shannon, C. E.: Communication in the Presence of Noise, Proceedings of the IRE, 37(1), pp. 10-21, 1949.

Slunyaev, A.: Nonlinear analysis and simulations of measured freak wave time series, European J. of Mechanics B / Fluids 25, 621-635, 2006.

Slunyaev, A.V.: Analysis of the nonlinear spectrum of intense sea waves with the purpose of extreme wave prediction, Radiophysics and quantum electronics, 61, 1-21, 2018.

Slunyaev, A.V.: Persistence of hydrodynamic envelope solitons: detection and rogue wave occurrence, Physics of Fluids, 33, 036606, 2021.

Stansell, P., Wolfram, J., and Linfoot, B.: Effect of sampling rate on wave height statistics, Ocean Engineering, 29 (9), 1023-1047, https: //doi.org/10.1016/s0029-8018(01)00066-x, 2002.

Sugavanam, S., Kopae, M. K., Peng, J. et al.: Analysis of laser radiation using the Nonlinear Fourier transform, Nat. Commun. 10, 5663, https://doi.org/10.1038/s41467-019-13265-4, 2019.

Tayfun, M.A. and Fedele, F.: Wave-height distributions and nonlinear effects, Ocean Eng. 34, 1631-1649, 2007.

Zabusky, N. J. and Kruskal, M. D.: Interaction of "Solitons" in a Collisionless Plasma and the Recurrence of Initial States, Physical Review Letters, Volume 15, pp. 240-243, 1965.

Zheng, Y., Lin, Z., Li, Y., Adcock, T., Li, Y., and Van Den Bremer, T.: Fully nonlinear simulations of unidirectional extreme waves provoked by strong depth transitions: The effect of slope, Phys. Rev. Fluids 5, 2020.

Zou, L., Wang, A., Wang, Z., Pei, Y., and Liu, X.: Experimental study of freak waves due to three-dimensional island terrain in random wave, Acta Oceanologica Sinica 38, 92-99, 2019.